

doi: 10.12029/gc20220421

尚永明,李小伟,祝新友,邹滔,黄行凯,程细音,王力,王树星. 2022. 内蒙古赤峰五十家子岩体成因及其对岩石圈伸展减薄的指示[J]. 中国地质, 49(4): 1323–1345.

Shang Yongming, Li Xiaowei, Zhu Xinyou, Zou Tao, Huang Xingkai, Cheng Xiyin, Wang Li, Wang Shuxing. 2022. Petrogenesis and its implications for the lithospheric thinning of the Wushijiazi pluton in Chifeng, Inner Mongolia[J]. Geology in China, 49(4): 1323–1345(in Chinese with English abstract).

内蒙古赤峰五十家子岩体成因 及其对岩石圈伸展减薄的指示

尚永明^{1,2}, 李小伟¹, 祝新友², 邹滔², 黄行凯², 程细音², 王力¹, 王树星³

(1. 中国地质大学(北京), 北京 100083; 2. 北京矿产地质研究院, 北京 100012;
3. 山东省第一地质矿产勘察院, 山东 济南 250014)

提要:【研究目的】内蒙古赤峰五十家子岩体位于大兴安岭南段成矿带的西南部, 对其进行系统的年代学和地球化学研究有助于丰富对区域构造–岩浆演化和成矿规律的认识。【研究方法】本文基于岩石学与地球化学研究工作, 采用LA-ICP-MS锆石U-Pb测年、主微量元素分析和锆石Lu-Hf同位素测试等方法分析了岩体成因。【研究结果】LA-ICP-MS锆石U-Pb测年结果表明, 五十家子岩体中的斑状含黑云母二长花岗岩、斑状含黑云母正长花岗岩和斑状黑云母正长花岗岩分别形成于(150.3±1.3) Ma, (145.9±1.8) Ma 和(137.1±2.2) Ma, 属晚侏罗世至早白垩世的产物。地球化学组成上, 该花岗岩体具有富硅、富碱、低铝、低钙的特点, 属于碱性、准铝质–弱过铝质A型花岗岩。锆石Hf同位素分析结果显示斑状含黑云母正长花岗岩具有正的 $\varepsilon_{\text{Hf}}(t)$ 值(+7.5~+14.3) 和年轻的二阶段模式年龄($t_{\text{DM2}}=285\sim718$ Ma), 与大兴安岭南段晚中生代花岗岩 $\varepsilon_{\text{Hf}}(t)$ 值相近, 表明其源区物质中年轻下地壳的贡献占主导地位, 斑状含黑云母二长花岗岩中暗色包体的发育指示其可能经历了岩浆混合作用。【结论】根据本文研究结果, 结合区域地质背景, 五十家子岩体可能形成于晚中生代岩石圈伸展减薄环境下, 软流圈上涌导致年轻下地壳发生部分熔融形成初始岩浆, 并与幔源岩浆混合, 后经高程度分异演化并于浅部侵位, 最终固结形成了五十家子花岗岩体。五十家子岩体具有显著的高分异和深源浅侵位特征, 与区域内锡多金属成矿作用有密切的成因联系。

关 键 词:中生代; A型花岗岩; 年代学; 地球化学; 地质调查工程; 内蒙古

创 新 点:采用LA-ICP-MS锆石U-Pb测年方法获取五十家子岩体3个岩相的形成时间, 依据岩相学特征、成岩时间、地球化学特征、锆石Hf同位素特征及区域地质背景综合分析岩体成因。

中图分类号:P588.121 **文献标志码:**A **文章编号:**1000-3657(2022)04-1323-23

Petrogenesis and its implications for the lithospheric thinning of the Wushijiazi pluton in Chifeng, Inner Mongolia

SHANG Yongming^{1,2}, LI Xiaowei¹, ZHU Xinyou², ZOU Tao², HUANG Xingkai²,

收稿日期:2019-03-21; 改回日期:2019-12-11

基金项目:国家重点研发计划“深地资源勘查开采”重点专项(2017YFC0601305, 2017YFC0602403)、国家自然科学基金项目(41602098)及中国地质调查局项目(DD20160072)联合资助。

作者简介:尚永明,男,1994年生,硕士生,主要从事岩浆作用与资源环境研究工作;E-mail: shangyongming@outlook.com。

通讯作者:祝新友,男,1965年生,教授级高级工程师,主要从事矿床学研究工作;E-mail: zhuxinyou@outlook.com。

CHENG Xiyin², WANG Li¹, WANG Shuxing³

(1. China University of Geosciences (Beijing), Beijing 100083, China; 2. Beijing Institute of Geology for Mineral Resources, Beijing 10001, China ; 3. No.1 Institute of Geology and Mineral Resources of Shandong Province, Jinan 250014, Shandong, China)

Abstract: This paper is the result of geological survey engineering.

[Objective] The Wushijiazi pluton in Chifeng area, Inner Mongolia, is located in the southwestern part of the metallogenic belt of the southern Great Xing'an Range. A systematic geochronological and geochemical study can provide insights into understanding of regional tectonic–magmatic evolution and metallogenic regularity. **[Methods]** Based on the petrological and geochemistry study, this paper uses LA–ICP–MS zircon U–Pb dating, major and trace element analysis and Zircon Hf isotopic analysis methods to analyze the genesis of the pluton. **[Results]** LA–ICP–MS zircon U–Pb dating results show that the porphyritic biotite–bearing monzogranite, porphyritic biotite–bearing syenogranite and porphyritic biotite syenogranite in the Wushijiazi pluton were formed at (150.3±1.3) Ma, (145.9±1.8)Ma and (137.1±2.2)Ma, respectively, which are the magmatic products during the Late Jurassic to Early Cretaceous. The pluton is geochemically characterized by high contents of silica and alkalis, but low contents of aluminium and calcium, belonging to alkaline and quasi aluminous–weakly peraluminous A–type granites. Zircon Hf isotopic analysis displays that the porphyritic biotite–bearing syenogranite has positive $\varepsilon_{\text{Hf}}(t)$ values (+7.5–+14.3) and juvenile two–stage (t_{DM2}) Hf model ages ($t_{\text{DM2}}=285–718$ Ma), which was consistent with those of Late Mesozoic granites in the southern of Great Xingan Range. Therefore, it is suggested that the contribution of the juvenile lower crust is dominant in the source region. The occurrence of mafic microgranular enclaves in porphyritic biotite – bearing monzogranite indicates magma critical role of mantle–crust interaction. **[Conclusions]** Combined with regional geological background, our study suggests that the asthenosphere upwelling resulted in partial melting of the juvenile lower crust and formed the primitive magma mush under the late Mesozoic lithospheric extension and thinning environment, and then the magma mush mixed with the mantle–derived magma. The highly fractionated mixed magma was emplaced in the shallow level, and finally formed the Wushijiazi granitic pluton. Wushijiazi pluton is characterized by the high degree of differentiation, as well as deep–source but shallow–emplacement, which is closely related to the tin–polymetallic mineralization in this area.

Key words: Mesozoic; A–type granite; geochronology; geochemistry; geological survey engineering; Inner Mongolia

Highlights: The formation time of the three lithofacies of the Wujipluton was obtained by LA–ICP–MS zircon U–Pb dating method, and the genesis of the pluton was comprehensively deciphered according to the petrographic characteristics, diagenetic time, geochemical characteristics, zircon Hf isotope characteristics and regional geological background.

About the first author: SHANG Yongming, male, born in 1994, master candidate, engaged in magmatism and mineral resources–environment; E–mail: shangyongming@outlook.com.

About the corresponding author: ZHU Xinyou, male, born in 1965, professorate senior engineer, engaged in mineral geology; E–mai: zhuxinyou@outlook.com.

Fund support: Supported by Subjects of Key Special Projects of National Key R&D Program "Exploration and Exploitation of Deep Earth Resources" (No. 2017YFC0601305, No. 2017YFC0602403), National Natural Science Foundation of China (No. 41602098), the Project of China Geological Survey (No. DD20160072).

1 引言

大兴安岭南段地区是中国最重要的有色金属产地之一,也是中国北方唯一成型的锡多金属成矿带(赵一鸣等, 2004)。区内分布有大量Sn–Pb–Zn–Ag–Cu多金属矿床,如大井锡铜多金属矿床、黄岗梁铁锡矿床、拜仁达坝铅锌银矿床、花敖包特铅锌矿床、浩布高铅锌矿床、白音诺尔铅锌矿床、布金黑

铅锌矿床和道伦达坝铜钨多金属矿床等(姚磊等, 2017; 张雪冰, 2017)。特别是近年来维拉斯托和白音查干两个大型锡多金属矿的相继发现,使得大兴安岭南段地区显示出巨大的锡成矿潜力。前人对区内锡多金属矿成矿地质体成因机制的研究十分关注,认为广泛分布的中生代花岗岩类与该区大规模内生成矿作用有着密切的成因联系(陈志广等, 2008)。然而,由于区域演化上历经古亚洲洋、蒙古

—鄂霍茨克洋及古太平洋三大构造体系的复合叠加,近年来相关学者对中生代大兴安岭南段地区大规模成岩成矿事件的构造背景及动力学机制认识存在较多争论,目前主要有以下几种主流观点:太平洋板块西向俯冲(Wakita et al., 2005; Mao et al., 2010; Zhang et al., 2010; Shu et al., 2016);蒙古—鄂霍茨克洋南向俯冲(Wang et al., 2002),或兴蒙造山带的造山后演化(Fan et al., 2003; 林强等, 2004);以及板内伸展背景下软流圈上涌等(邵济安等, 2001b)。同时,大兴安岭南段地区广泛发育的中生代高分异花岗岩类的成因类型及其与锡多金属成矿的密切联系也引起了广泛关注和讨论(祝新友等, 2016; 管育春等, 2017; 李真真等, 2019)。

前人对五十家子岩体南部的哈什吐钼矿床研究较多,主要集中于矿床及赋矿岩体的年代学、成因等(翟德高等, 2012; 张可等, 2012; Zhai et al., 2014, 2017; Ding et al., 2016),而对高度分异演化的花岗岩体特征与岩体内锡多金属成矿之间的成因联系的研究相对较少。此外,前人对五十家子岩体中花岗岩成因类型的认识尚存在争议,Zhai et al. (2014)研究认为其属于A型花岗岩,而万乐等(2016)将其判定为I型花岗岩。本文重点对五十家子岩体开展系统的岩相学、同位素年代学、地球化学分析工作,结合已有的地球化学、年代学成果,对其岩浆演化过程及其与成矿的确切关系进行了研究,同时对大兴安岭南段地区晚中生代时期构造—岩浆—成矿大爆发现象的动力学背景进行了初步探讨,以为该区锡多金属成矿机制的深入研究提供依据,并为区内进一步找矿工作提供线索。

2 地质背景

五十家子岩体位于大兴安岭南段。大地构造位置位于西伯利亚板块和华北板块之间的缝合造山带(中亚造山带)东端的兴蒙造山带内,区域构造隶属于松辽—锡林浩特地块中部,西里庙—达青牧场大断裂与大兴安岭主脊断裂的中间部位。区域上断裂构造十分发育,主要经历了海西期和燕山期构造运动的叠加作用,形成了棋盘状纵横交错的断裂系统,以北东向断裂构造为主,北西向及东西向断裂构造次之。受区域性深大断裂影响,区内岩浆活动强烈且分布广泛,继海西期中基性岩浆活动峰

期之后,尤以燕山期大规模的中酸性岩浆侵入和喷发活动最为显著,形成的岩体多呈岩株、岩脉或岩基形式。多期构造—岩浆活动形成的复杂断裂系统和丰富的岩浆岩对成矿物质的迁移、富集和沉淀成矿都极为有利。因此,特殊的岩浆岩—构造组合形成和保存了区内丰富的锡多金属矿产资源。

研究区内出露的地层主要为二叠系大石寨组,主要岩性为碎屑岩夹少量碳酸盐岩;中侏罗统新民组,岩性主要为陆相酸性火山熔岩和碎屑岩;上侏罗统白音高老组、满克头鄂博组、土城子组,岩性为中酸性火山熔岩及碎屑岩;下白垩统梅勒图组,岩性为气孔状、杏仁状玄武岩或安山岩。

3 岩石学与岩相学特征

五十家子岩体位于林西县城北约45 km处,呈北东向分布(与区域构造线方向一致),呈椭圆状岩基产出。岩体规模较大,长约43 km,最宽处约20 km,出露面积约410 km²。岩体侵入二叠系砂板岩中,南侧为三叠纪花岗闪长岩带,北东侧为二叠纪西耳子黑云母二长花岗岩带,岩体侵入花岗闪长岩岩体及黑云母二长花岗岩岩体中,呈渐变侵入接触关系。花岗斑岩呈岩株状侵入五十家子岩体中部。五十家子岩体根据岩性组合特征可分为3个岩相,即含黑云母二长花岗岩相、含黑云母正长花岗岩相和斑状黑云母正长花岗岩相。

含黑云母二长花岗岩相,主要岩性为中细粒—中粒—斑状含黑云母二长花岗岩,局部过渡为含黑云母正长花岗岩,二者为渐变接触关系,主要分布于朝阳沟北部,该相带岩石中暗色微粒包体较为发育(图2a);含黑云母正长花岗岩相,主要岩性为细粒—中细粒—斑状含黑云母正长花岗岩,边部粒度较细,向内部粒度逐渐变粗,哈什吐一带可见斑状含黑云母正长花岗岩侵入含黑云母二长花岗岩中且具有截然界线(Ding et al., 2016),含黑云母正长花岗岩成环带状分布于毡铺—老房身一带(图1);斑状黑云母正长花岗岩相,主要岩性为细粒—中细粒斑状黑云母正长花岗岩,分布于朝阳沟一小乌兰一带,可见其呈岩枝状侵入到斑状含黑云母正长花岗岩中(图2b)。由各相带的相互接触关系,可知岩体侵位的顺序由早到晚分别为斑状含黑云母二长花岗岩、斑状含黑云母正长花岗岩、斑状黑云母正长

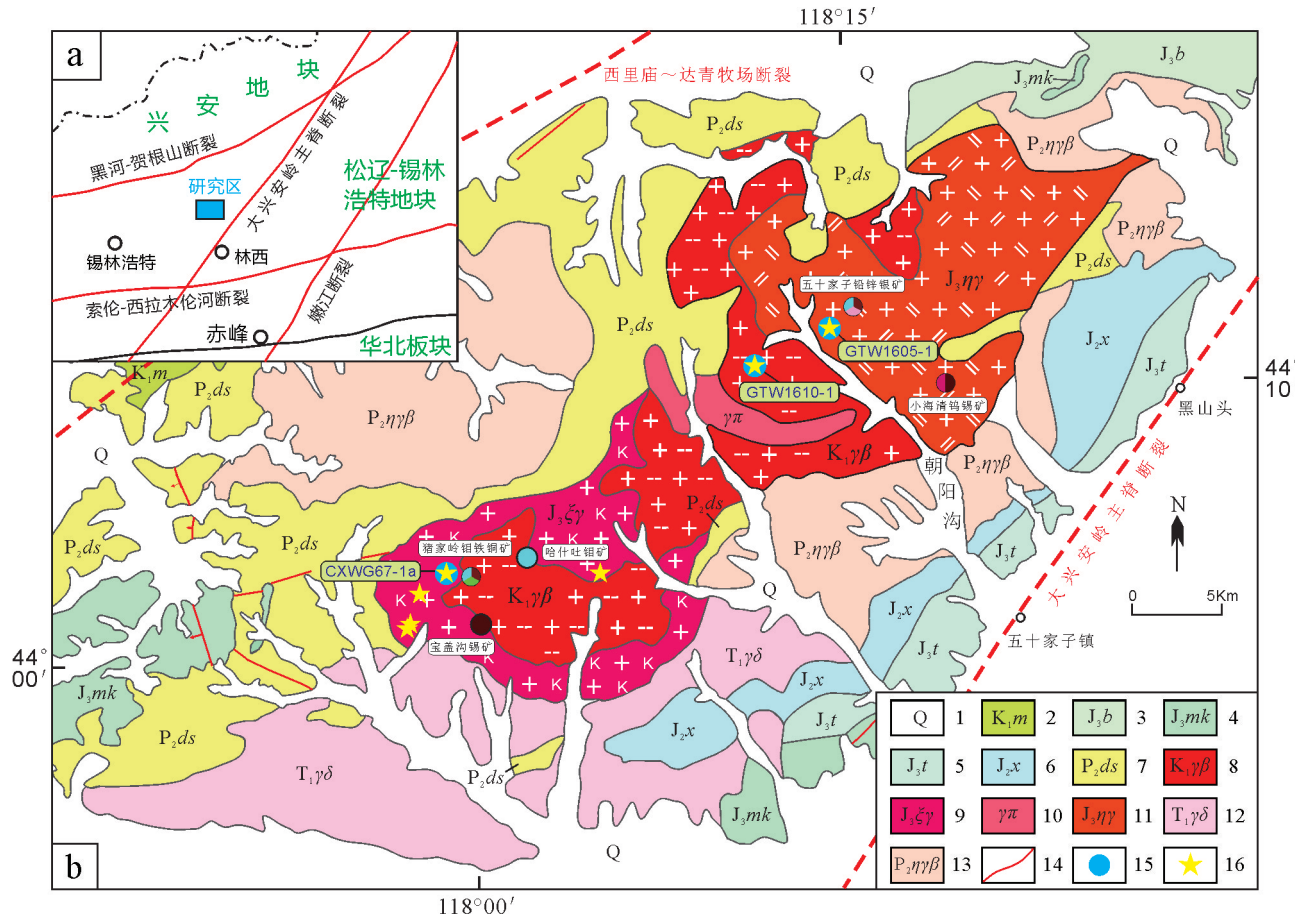


图1 五十家子区域地质图(a据Liu et al., 2017修改; b据1:25万地质图^①修改)

1—第四系; 2—下白垩统梅勒图组; 3—上侏罗统白音高老组; 4—上侏罗统满克头鄂博组; 5—上侏罗统土城子组; 6—中侏罗统新民组; 7—下二叠统大石寨组; 8—早白垩世斑状黑云母正长花岗岩; 9—晚侏罗世含黑云母正长花岗岩; 10—花岗斑岩; 11—晚侏罗世含黑云母二长花岗岩; 12—晚二叠世花岗闪长岩; 13—晚二叠世黑云母二长花岗岩; 14—断裂; 15—年龄采样点; 16—地球化学采样点

Fig.1 Geological map of the Wushijiazi area (a, modified after Liu et al., 2017; b, modified after 1:250000 geological map^①)
1—Quaternary; 2—Lower Cretaceous Meiletu Formation; 3—Upper Jurassic Baiyingaolao Formation; 4—Upper Jurassic Manketouebo Formation; 5—Upper Jurassic Tuchengzi Formation; 6—Middle Jurassic Xinmin Formation; 7—Lower Permian Dashizhai Formation; 8—Early Cretaceous porphyritic biotite syenogranite; 9—Late Jurassic biotite-bearing syenogranite; 10—Granite porphyry; 11—Late Jurassic biotite-bearing monzogranite; 12—Late Permian granodiorite; 13—Late Permian biotite monzogranite; 14—Fault; 15—Age sampling location; 16—Geochemical sampling location

花岗岩,这也得到了锆石U-Pb测年结果的支持(依次为 (150.3 ± 1.3) Ma, (145.9 ± 1.8) Ma, (137.1 ± 2.2) Ma)。该岩体各岩相中均可见伟晶岩脉、细晶岩脉发育,而晶洞构造在斑状含黑云母正长花岗岩和斑状黑云母正长花岗岩中较为常见。

根据野外及镜下岩矿鉴定,由样品中主要矿物含量划分的岩石类型见表1和图2。

斑状含黑云母二长花岗岩,岩石新鲜面呈灰白色,似斑状结构,块状构造。斑晶含量30%~35%,由条纹长石(10%~15%),石英(约10%),斜长石(约10%)组成;基质含量65%~70%,主要由条纹长石

(20%~25%)、石英(约20%)、斜长石(约20%)以及少量黑云母(约5%)组成,条纹长石多发生高岭土化,斜长石自形程度较高,发育聚片双晶,部分可见筛状变晶结构,副矿物主要为锆石、磷灰石、磁铁矿等(图4a、b)。

斑状含黑云母正长花岗岩,岩石新鲜面呈浅肉红色,似斑状结构,块状构造。斑晶含量35%~40%,矿物组成为条纹长石(约25%),石英(10%~15%);基质含量60%~65%,由条纹长石(25%~30%)、石英(约22%)、斜长石(约10%)及黑云母(约3%)组成,条纹长石多发生高岭土化,斜长石可见聚片双晶,

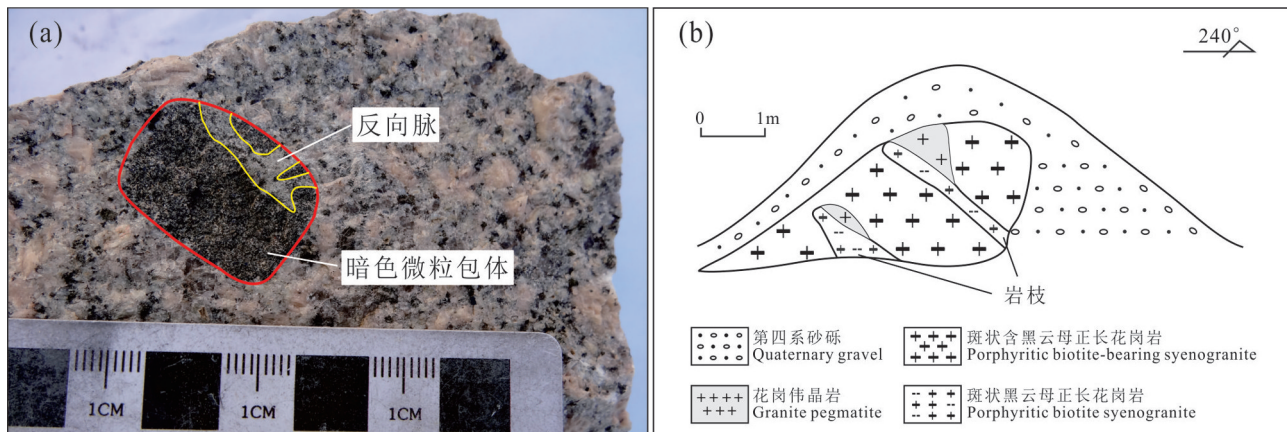


图2五十家子岩体中暗色包体照片(a)和岩相接触关系地质简图(b)

Fig.2 Field photographs of microgranular enclaves (a) and geological sketch map of contacting relationship (b) of the Wushijiazi pluton

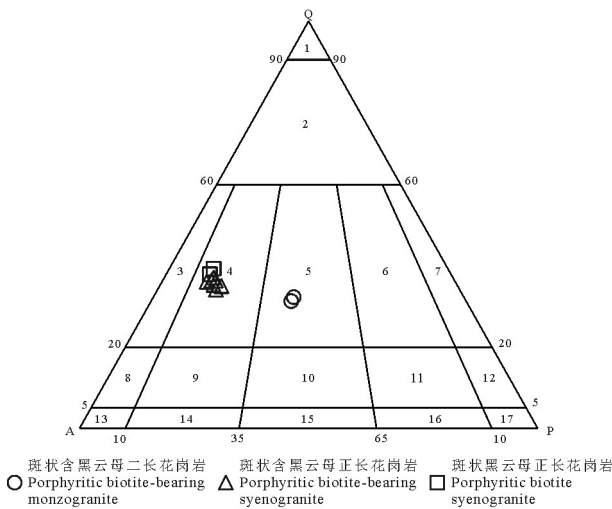


图3五十家子岩体QAP图解

1—硅英岩(英石岩);2—富石英花岗岩;3—碱长花岗岩;4—正长花岗岩;5—二长花岗岩;6—花岗闪长岩;7—莫云闪长岩;8—石英碱长正长岩;9—石英正长岩;10—石英二长岩;11—石英二长闪长岩或石英二长辉长岩;12—石英闪长岩,石英辉长岩或石英斜长岩;13—碱长正长岩;14—正长岩;15—二长岩;16—二长闪长岩或二长辉长岩;17—闪长岩,辉长岩或斜长岩

Fig.3 QAP diagram of the Wushijiazi pluton

1—Quartzolite; 2—Quartz-rich granitoid; 3—Alkali feldspar granite; 4—Syenogranite; 5—Monzogranite; 6—Granodiorite; 7—Tonalite; 8—Quartz alkali feldspar syenite; 9—Quartz syenite; 10—Quartz monzonite; 11—Quartz monzodiorite or quartz monzogabbro; 12—Quartz diorite, quartz gabbro or quartz anorthositic; 13—Alkali feldspar syenite; 14—Syenite; 15—Monzonite; 16—Monzodiorite or monzogabbro; 17—Diorite, gabbro or anorthosite

副矿物主要为磷灰石、锆石等(图4c、d)。

斑状黑云母正长花岗岩,岩石新鲜面呈浅肉红色,似斑状结构,块状构造。斑晶含量20%~25%,矿

物组成为条纹长石(约10%),石英(5%~10%),黑云母(约4%)及少量斜长石(约1%);基质含量75%~80%,由条纹长石(约35%)、石英(约25%)、斜长石(约8%)及黑云母(7%~12%)组成,条纹长石见有高岭土化,斜长石发育聚片双晶,可见绢云母化,石英多为烟灰色,副矿物主要为磷灰石、锆石等(图4e、f)。

4 样品采集与分析方法

所有测试样品均取自五十家子岩体新鲜露头,采样位置见图1。其中GTW1605-1、HTW1605-1a、HTW1605-1b岩性为斑状含黑云母二长花岗岩,CXWC62-1a、CXWC62-1b、CXWC63-1、CXWC65-1、CXWG67-1a、CXWC67-1a、CXWC67-1b、CXWC69-1为斑状含黑云母正长花岗岩,GTW1610-1、HTW1610-1a、HTW1610-1b为斑状黑云母正长花岗岩。

在避免污染的条件下,将用于锆石年代学测试的样品粉碎至60目以下,先经重液分离及磁选进行锆石单矿物粗选,然后在双目镜下将晶形完好、色泽及透明度良好的锆石单矿物逐粒挑出,黏于环氧树脂表面进行抛光处理,并将处理后的待测锆石进行透射光、反射光显微照相,据此选择晶体特征良好的样品(避开锆石内部包裹体及裂隙),进行阴极发光(CL)拍照,最后根据CL图像显示的锆石内部结构特征,进一步选择典型的岩浆锆石进行U-Pb测年分析。锆石靶的制定和阴极发光(CL)照相均在北京锆年领航科技有限公司进行。

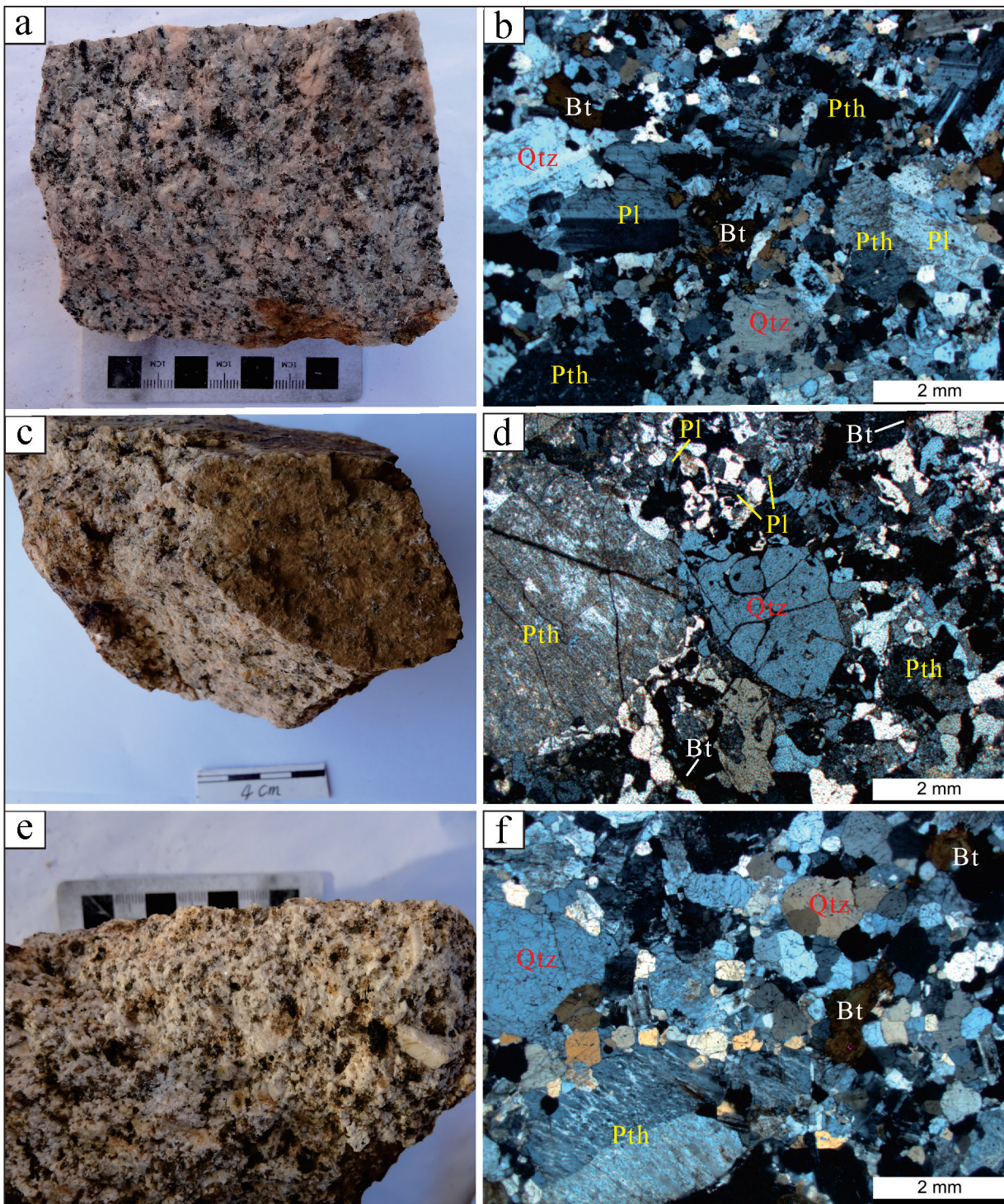


图4 五十家子岩体的手标本及镜下特征

a, b—斑状含黑云母二长花岗岩及其镜下照片; c, d—斑状含黑云母正长花岗岩及其镜下照片; e, f—斑状黑云母正长花岗岩及其镜下照片;
b、d、f均为正交偏光; Pl—斜长石; Qtz—石英; Pth—条纹长石; Bt—黑云母

Fig.4 Hand specimens and microscopic features of the Wushijiazi pluton

a, b—Hand specimen and microscopic feature of porphyritic biotite-bearing monzogranite; c, d—Hand specimen and microscopic feature of porphyritic biotite-bearing syenogranite; e, f—Hand specimen and microscopic feature of porphyritic biotite syenogranite; b, d, f are crossed nicols; Pl—Plagioclase; Qtz—Quartz; Pth—Perthite; Bt—Biotite

表1 五十家子岩体主要长英质矿物(QAP)含量
Table 1 Major mineral composition (QAP) of the Wushijiazi pluton

样品号	岩性	矿物含量/%		
		Q	A	P
BTW1605-1a	斑状含黑云母二长花岗岩	31	38	31
BTW1605-1b	斑状含黑云母二长花岗岩	32	37	31
CXWC62-1a	斑状含黑云母正长花岗岩	34	53	13
CXWC62-1b	斑状含黑云母正长花岗岩	35	52	14
CXWC63-1	斑状含黑云母正长花岗岩	35	53	12
CXWC65-1	斑状含黑云母正长花岗岩	36	52	12
CXWG67-1a	斑状含黑云母正长花岗岩	36	54	10
CXWC67-1a	斑状含黑云母正长花岗岩	36	53	11
CXWC67-1b	斑状含黑云母正长花岗岩	37	52	11
CXWC69-1	斑状含黑云母正长花岗岩	36	53	11
HTW1610-1a	斑状黑云母正长花岗岩	38	53	10
HTW1610-1b	斑状黑云母正长花岗岩	39	51	10

注:以实际矿物含量为基础,QAP含量总和为100%。

锆石U-Pb定年在合肥工业大学资源与环境工程学院质谱实验室进行。实验采用激光剥蚀电感耦合等离子质谱分析(LA-ICP-MS)技术。ICP-MS为美国Agilent公司生产的Agilent7500a,激光剥蚀系统为美国Coherent Inc.公司生产的GeoLasPro,该系统工作波长为193 nm,束斑直径大小为4~160 μm可调,能量密度范围1~45 J/cm²,单脉冲能量可达200 mJ,最高重复频率20 Hz。采用He作为剥蚀物质的载气,采用国际标准锆石91500作为外部锆石年龄标样,采用NIST SRM 610玻璃标样作为元素外标进行同位素分馏校正。实验中锆石年龄分析采用的激光束斑直径为30 μm,激光频率为8 Hz,能量密度为6 J/cm²。样品的同位素数据采用中国地质大学(武汉)研发的ICPMsDataCal(V10.7版)软件进行数据处理并成图,普通铅校正采用Andersen(2002)的方法,锆石加权年龄的计算及谐和图的绘制采用Ludwig(2003)的ISOPLT(Version 3.00)进行,实验过程中误差为1σ。

主量元素和微量元素分析测试在核工业北京地质研究院分析测试研究中心完成。主量元素通过X射线荧光光谱仪测定,仪器型号为飞利浦PW2404,样品测试方法参考GB/T14506.28-93《硅酸盐岩石化学分析方法X射线荧光光谱法测定主、次元素量》。微量元素的分析采用高分辨电感耦合等离子质谱法,测试的仪器型号为Finnigan MAT制

造,HR-ICP-MS(Element I),样品测试参考DZ/T0223-2001电感耦合等离子体质谱(ICP-MS)方法通则。

锆石微区原位Lu-Hf同位素测试在西北大学大陆动力学国家重点实验室完成。Lu-Hf分析采用的仪器为Nu Instrument公司生产的多接收等离子质谱仪(Nu Plasma II MC-ICP-MS),激光剥蚀系统采用193 nm准分子激光剥蚀系统(RESolutionM-50,ASI),锆石Hf同位素测试在原年龄测点附近进行,测试过程中,激光能量密度为6 J/cm²,频率为5 Hz,斑束直径为44 μm,采用高纯度He作为载气,以91500和Mudtank作为监控样品,具体仪器配置及分析流程参考文献(Yuan et al., 2008)。 $\varepsilon_{\text{Hf}}(t)$ 的计算依据所测锆石U-Pb年龄,采用的¹⁷⁶Lu衰变常数为 1.867×10^{-11} a (Albarède et al., 2006),采用球粒陨石的¹⁷⁶Hf/¹⁷⁷Hf为0.282772,¹⁷⁶Lu/¹⁷⁷Hf为0.0332 (Blicherttoft and Albarède, 1997),Hf同位素一阶段模式年龄的计算采用现今亏损地幔的¹⁷⁶Hf/¹⁷⁷Hf和¹⁷⁶Lu/¹⁷⁷Hf比值,其中¹⁷⁶Hf/¹⁷⁷Hf = 0.28325,¹⁷⁶Lu/¹⁷⁷Hf = 0.0384 (Griffin et al., 2000)。二阶段Hf同位素模式年龄的计算时采用的平均地壳的¹⁷⁶Lu/¹⁷⁷Hf值为0.015 (Rudnick and Gao, 2003)。

5 分析结果

5.1 年代学

五十家子岩体LA-ICP-MS锆石U-Pb测年结果见表2,年代学样品位置及编号见图1。五十家子斑状含黑云母二长花岗岩锆石多呈长柱状,长100~200 μm,宽50~110 μm,晶形基本完好,阴极发光下均具有清晰的振荡环带结构(图5)。锆石的Th/U比值变化于0.25~0.73,其²⁰⁶Pb/²³⁸U加权平均年龄为(150.3 ± 1.3) Ma (n=9, MSWD = 2.8)(图6),属晚侏罗世产物。斑状含黑云母正长花岗岩锆石多呈短柱状,长150~300 μm,宽60~160 μm,晶形基本完好,阴极发光下均具有清晰的振荡环带结构(图5)。锆石的Th/U比值为0.39~2.08,其²⁰⁶Pb/²³⁸U加权平均年龄为(145.9 ± 1.8) Ma (n=16, MSWD = 4.1)(图6),属晚侏罗世产物。斑状黑云母正长花岗岩锆石多呈长柱状,长130~230 μm,宽50~130 μm,晶形较好,阴极发光下均具有清晰的振荡环带结构(图5)。锆石的Th/U比值变化于0.24~0.78,其²⁰⁶Pb/²³⁸U加权平均年龄为

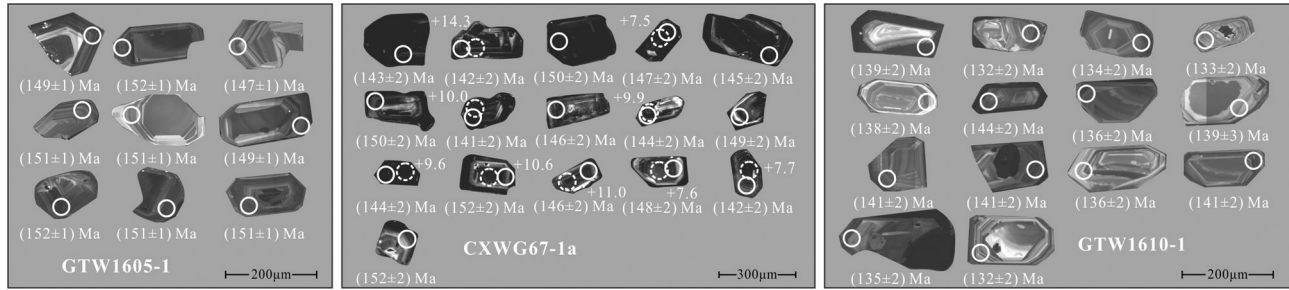


图5 五十家子岩体锆石CL阴极发光图像
(实线为锆石U-Pb测试点,虚线为Hf同位素测试点)

Fig.5 Cathodoluminescence images of zircons of the Wushijiazi pluton
(The solid line is zircon U-Pb test point, and the dotted line is Hf isotope test point)

(137.1 ± 2.2) Ma ($n=14$, MSWD = 3.5)(图6),属早白垩世产物。在 $^{206}\text{Pb}/^{238}\text{U}$ - $^{207}\text{Pb}/^{235}\text{U}$ 谐和图上,本次所测样品点存在沿水平方向不同程度偏离谐和线现象(图6),一方面可能因为年轻锆石中 ^{207}Pb 丰度低而造成的测试数据误差,另一方面可能与锆石中的微量普通铅有关(Yuan et al., 2003)。而当前年轻锆石定年主要采用精度较高的 $^{206}\text{Pb}/^{238}\text{U}$ 年龄,这种水平漂移现象不会对定年结果产生显著影响(邱检生等,2008),因此本次所测定数据可以准确反映岩体的成岩年龄。锆石测年结果表明,岩体由早到晚侵位的顺序为斑状含黑云母二长花岗岩、斑状含黑云母正长花岗岩、斑状黑云母正长花岗岩,为3个阶段侵入的产物。

5.2 地球化学

5.2.1 主量元素特征

五十家子花岗岩体主微量元素分析结果见表3。主量元素组成上有以下特征:(1)富硅, SiO_2 含量在71.36%~76.91%,平均值为74.89%,高于中国花岗岩和兴蒙造山带花岗岩平均含量(分别为72.20%和

72.73%,史长义等,2005),而与南岭31个钨锡成矿花岗岩的平均含量(74.63%,祝新友等,2016)相当,且岩体分异指数(DI)在89.07~97.11间。(2)低铝, Al_2O_3 含量为12.31%~15.34%,平均值13.25%,A/CNK-A/NK关系图显示样品岩石属于准铝一弱过铝质花岗岩(图7a)。(3)富碱,全碱($\text{K}_2\text{O}+\text{Na}_2\text{O}$)含量为7.74%~9.04%,平均值8.50%,且相对富钾, $\text{K}_2\text{O}/\text{Na}_2\text{O}$ 比值介于1.09~1.34。岩石的碱铝指数(AKI)为0.72~0.93,碱度率指数(AR)为2.58~4.99,在AR-SiO₂图中显示碱性系列特征(图7b)。(4)低钙、镁、钛、磷,五十家子花岗岩体的CaO、MgO、TiO₂、P₂O₅含量平均值分别为0.64%、0.14%、0.13%、0.04%,这一成分特点对岩石高度分异演化的特征同样有指示意义(邱检生等,2008)。因此,总体上五十家子花岗岩体是一套具有富硅、富碱、低铝、低钙等特点的岩石组合,这与A型花岗岩特征一致(陈建林等,2004)。

5.2.2 微量元素特征

在微量元素原始地幔标准化蜘蛛图中(图8b),五十家子花岗岩体各岩相不同程度的富集Rb、Th、

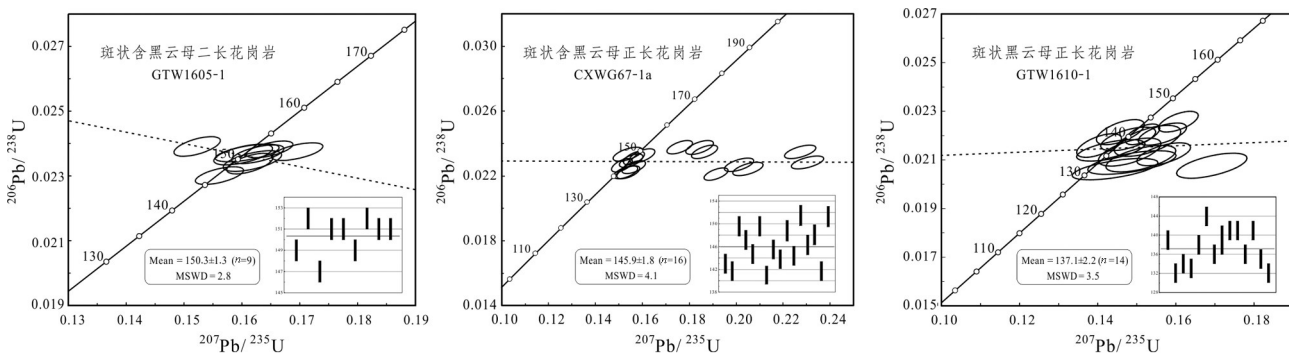


图6 五十家子岩体锆石U-Pb年龄及谐和图

Fig.6 LA-ICP-MS zircon U-Pb concordia and weighted average diagrams of the Wushijiazi pluton

表2 五十家子岩体LA-ICP-MS锆石U-Pb分析结果
Table 2 LA-ICP-MS zircon U-Pb analyses for the Wushijiazi pluton

测点号	同位素比值										年龄/Ma					
	含量/ 10^{-6}	Th	U	Th/U	$^{207}\text{Pb}/^{206}\text{Pb}$	1 σ	$^{207}\text{Pb}/^{235}\text{U}$	1 σ	$^{206}\text{Pb}/^{238}\text{U}$	1 σ	$^{207}\text{Pb}/^{206}\text{Pb}$	1 σ	$^{207}\text{Pb}/^{235}\text{U}$	1 σ	$^{206}\text{Pb}/^{238}\text{U}$	1 σ
GTW1605-1																
1	381	1269	0.30	0.04994	0.00065	0.16139	0.00264	0.02338	0.00021	192	22	152	2	149	1	
2	564	1303	0.43	0.05011	0.00072	0.16478	0.00267	0.02382	0.00017	200	24	155	2	152	1	
3	265	676	0.39	0.04920	0.00080	0.15612	0.00275	0.02301	0.00018	157	27	147	2	147	1	
4	178	580	0.31	0.04913	0.00094	0.16023	0.00335	0.02366	0.00021	154	32	151	3	151	1	
5	215	435	0.49	0.04934	0.00112	0.16092	0.00364	0.02371	0.00018	164	39	152	3	151	1	
6	220	597	0.37	0.05005	0.00098	0.16182	0.00334	0.02346	0.00021	197	32	152	3	149	1	
7	675	921	0.73	0.04618	0.00074	0.15227	0.00265	0.02391	0.00020	7	23	144	2	152	1	
8	285	1130	0.25	0.04989	0.00090	0.16276	0.00298	0.02367	0.00019	190	28	153	3	151	1	
9	598	1625	0.37	0.05153	0.00079	0.16956	0.00294	0.02375	0.00018	265	26	159	3	151	1	
CXWG67-1a																
1	183	723	0.25	0.06623	0.00181	0.20491	0.00428	0.02243	0.00027	814	56	189	4	143	2	
2	323	918	0.35	0.04986	0.00140	0.15284	0.00335	0.02222	0.00026	189	64	144	3	142	2	
3	407	1103	0.37	0.05758	0.00151	0.18653	0.00364	0.02348	0.00027	513	57	174	3	150	2	
4	491	1378	0.36	0.04911	0.00126	0.15648	0.00295	0.02310	0.00027	153	59	148	3	147	2	
5	297	898	0.33	0.06426	0.00175	0.20121	0.00415	0.02270	0.00027	750	56	186	4	145	2	
6	406	901	0.45	0.07016	0.00184	0.22731	0.00441	0.02349	0.00028	933	53	208	4	150	2	
7	639	1631	0.39	0.06277	0.00155	0.19140	0.00333	0.02211	0.00025	700	52	178	3	141	2	
8	271	874	0.31	0.07314	0.00194	0.23037	0.00451	0.02283	0.00027	1018	53	211	4	146	2	
9	360	935	0.38	0.05025	0.00140	0.15633	0.00335	0.02255	0.00026	207	63	148	3	144	2	
10	213	620	0.34	0.04780	0.00151	0.15381	0.00409	0.02334	0.00029	88	74	145	4	149	2	
11	444	1232	0.36	0.04847	0.00126	0.15133	0.00298	0.02265	0.00027	122	60	143	3	144	2	
12	421	1044	0.40	0.05368	0.00142	0.17596	0.00358	0.02377	0.00028	358	59	165	3	152	2	
13	370	1068	0.35	0.04903	0.00132	0.15519	0.00325	0.02295	0.00027	149	62	147	3	146	2	
14	290	921	0.32	0.04986	0.00141	0.15982	0.00359	0.02324	0.00028	188	64	151	3	148	2	
15	331	960	0.34	0.05022	0.00136	0.15397	0.00323	0.02223	0.00026	205	62	145	3	142	2	
16	202	759	0.27	0.05626	0.00154	0.18433	0.00392	0.02375	0.00028	462	60	172	3	151	2	
GTW1610-1																
1	168	425	0.40	0.04884	0.00162	0.14779	0.00463	0.02186	0.00032	140	46	140	4	139	2	
2	336	868	0.39	0.05081	0.00264	0.14444	0.00723	0.02062	0.00029	232	121	137	6	132	2	
3	285	1031	0.28	0.05204	0.00222	0.15105	0.00590	0.02105	0.00036	287	100	143	5	134	2	
4	331	761	0.44	0.05165	0.00270	0.14876	0.00745	0.02089	0.00032	270	123	141	7	133	2	
5	333	875	0.38	0.04686	0.00128	0.14035	0.00378	0.02159	0.00032	42	35	133	3	138	2	
6	654	1866	0.35	0.05110	0.00102	0.16064	0.00335	0.02257	0.00028	246	26	151	3	144	2	
7	290	829	0.35	0.04861	0.00207	0.14335	0.00577	0.02139	0.00029	129	97	136	5	136	2	
8	81	309	0.26	0.05125	0.00193	0.15276	0.00560	0.02178	0.00042	252	50	144	5	139	3	
9	264	653	0.40	0.04784	0.00138	0.14579	0.00404	0.02214	0.00034	91	37	138	4	141	2	
10	259	1055	0.25	0.05150	0.00139	0.15657	0.00408	0.02206	0.00030	263	35	148	4	141	2	
11	129	441	0.29	0.05074	0.00186	0.14818	0.00528	0.02132	0.00038	229	50	140	5	136	2	
12	412	1301	0.32	0.04963	0.00102	0.15146	0.00293	0.02205	0.00028	178	23	143	3	141	2	
13	125	409	0.31	0.05377	0.00175	0.15689	0.00453	0.02123	0.00031	362	39	148	4	135	2	
14	200	401	0.50	0.05879	0.00203	0.16920	0.00594	0.02076	0.00034	559	48	159	5	132	2	

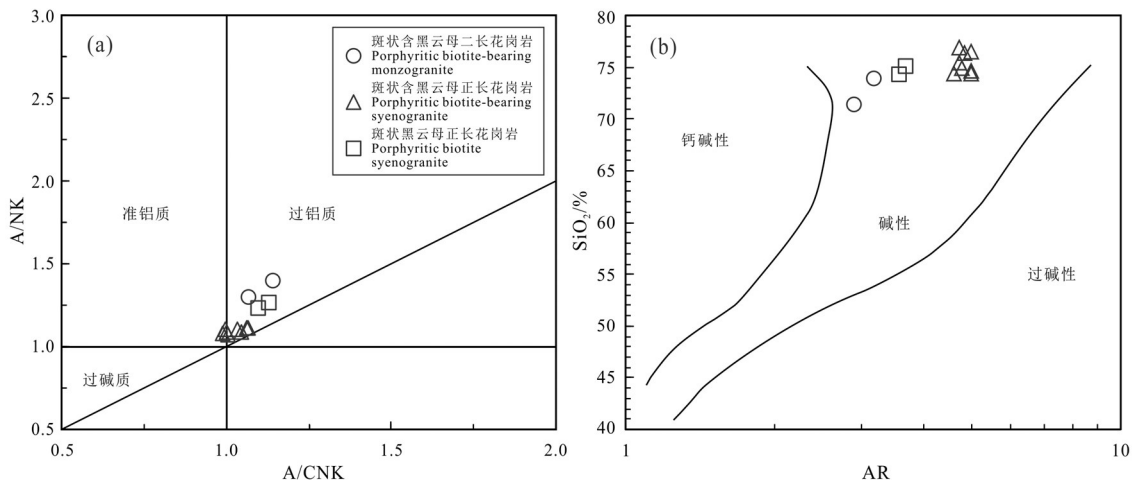


图7五十家子岩体的A/CNK-A/NK图解(a,据Maniard and Piccoli, 1989)和AR-SiO₂图解(b,据Wright, 1969)

Fig.7 A/CNK-A/NK (a, after Maniard and Piccoli, 1989) and AR-SiO₂ (b, after Wright, 1969) diagrams of the Wushijiazi pluton

Pb、Hf等元素,亏损Ba、Sr、P、Ti、Eu等元素。高场强元素Nb、Ta含量相对较低,而Zr、Hf相对富集,Nb/Ta介于4.41~13.72,远低于幔源岩浆Nb/Ta=17±1的比值(Hofmann, 1988; 汪洋, 2009; 周振华等, 2010)。Rb/Sr在2.20~24.53,Rb/Ba在0.64~5.18。

五十家子花岗岩体的ΣREE最高为285.73×10⁻⁶,平均值193.07×10⁻⁶,总体表现为稀土含量较高;(La/Yb)_N为2.05~9.19,显示轻稀土富集特征;(La/Sm)_N和(Gd/Yb)_N的比值分别为3.79~6.57和0.87~2.54,表明轻稀土较重稀土分馏程度更高;岩石的稀土元素球粒陨石标准化配分型式为右倾海

鸥型,δEu值变化于0.02~0.43,平均值0.15,显示铕亏损强烈(图8a);上述稀土元素含量特征及分布模式图与典型A型花岗岩的稀土元素配分型式相似(Eby, 1992; 鄢圣武等, 2017)。

5.2.3 锆石Hf同位素特征

锆石的结晶温度和Hf同位素封闭温度较高,是目前示踪岩浆源区特征、反演源区物质时限的有效手段(韦少港等, 2017)。本文选择五十家子岩体中的斑状含黑云母正长花岗岩锆石样品CXWG67-1a进行了Lu-Hf同位素测试,分析结果见表4。斑状含黑云母正长花岗岩的¹⁷⁶Hf/¹⁷⁷Hf比值较为均一,介

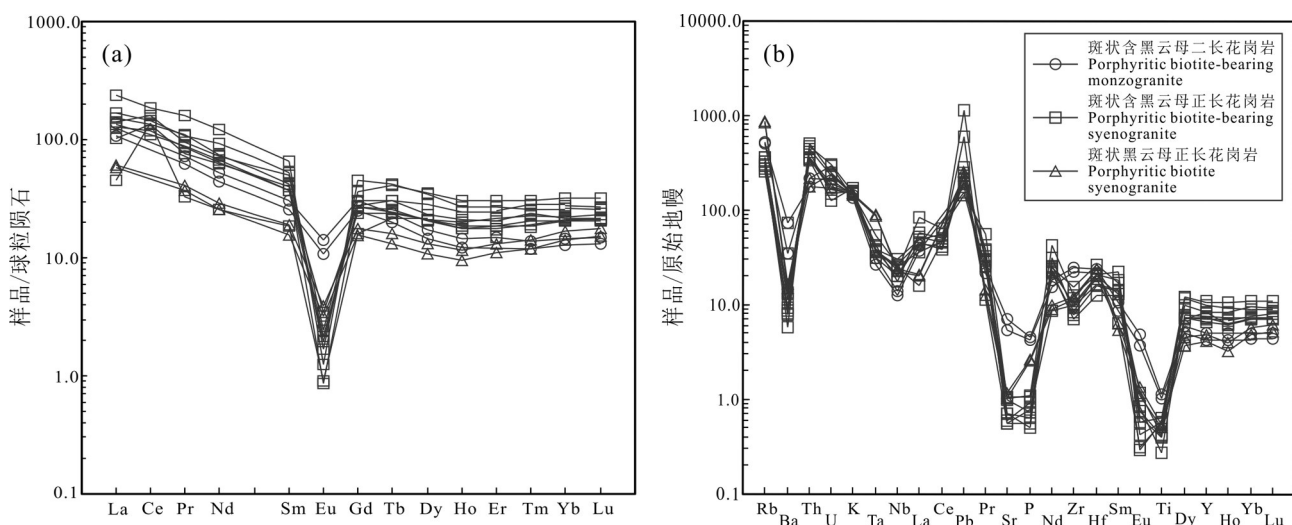


图8五十家子岩体的REE配分图(a)和微量元素蛛网图(b)(球粒陨石和原始地幔标准化值据Sun and McDonough, 1989)

Fig.8 Chondrite-normalized REE distribution patterns (a) and primitive mantle-normalized trace elements spidergrams (b) of the Wushijiazi pluton (chondrite and primitive mantle data after Sun and McDonough, 1989)

表3 五十家子岩体主要元素(%)和微量元素(10^{-6})组成

测试项目	HTW1605-1a HTW1605-1b CXWC62-1a CXWC62-1b CXWC63-1 CXWC65-1 CXWG67-1a CXWG67-1b CXWC69-1 HTW1610-1a HTW1610-1b		斑状含黑云母正长花岗岩		斑状黑云母正长花岗岩							
	斑状含黑云母二长花岗岩	斑状含黑云母正长花岗岩 ^b	CXWC62-1a CXWC63-1 CXWC65-1 CXWG67-1a CXWG67-1b CXWC69-1 HTW1610-1a HTW1610-1b 斑状黑云母正长花岗岩	CXWC62-1a CXWC63-1 CXWC65-1 CXWG67-1a CXWG67-1b CXWC69-1 HTW1610-1a HTW1610-1b 斑状黑云母正长花岗岩	CXWC62-1a CXWC63-1 CXWC65-1 CXWG67-1a CXWG67-1b CXWC69-1 HTW1610-1a HTW1610-1b 斑状黑云母正长花岗岩	CXWC62-1a CXWC63-1 CXWC65-1 CXWG67-1a CXWG67-1b CXWC69-1 HTW1610-1a HTW1610-1b 斑状黑云母正长花岗岩						
SiO ₂	73.89	71.36	74.75	74.39	74.47	74.98	76.91	76.51	76.46	75.48	75.12	74.32
TiO ₂	0.23	0.25	0.12	0.12	0.14	0.12	0.06	0.09	0.09	0.09	0.12	0.11
Al ₂ O ₃	13.58	15.34	13.05	13.30	13.26	12.78	12.36	12.31	12.31	12.89	13.51	14.22
Fe ₂ O ₃	0.28	0.33	1.11	1.12	0.55	1.19	0.16	0.35	0.22	0.77	0.48	0.39
FeO	1.90	1.99	0.64	0.42	0.75	0.46	0.97	0.91	0.92	0.56	1.03	0.99
MnO	0.04	0.04	0.03	0.02	0.01	0.01	0.01	0.01	0.01	0.03	0.03	0.03
MgO	0.28	0.34	0.09	0.09	0.10	0.08	0.07	0.08	0.08	0.11	0.20	0.21
CaO	1.23	1.35	0.28	0.29	0.71	0.57	0.43	0.44	0.60	0.32	0.70	0.72
Na ₂ O	3.68	3.82	4.18	3.87	4.10	4.03	3.85	4.07	3.93	3.97	3.87	3.85
K ₂ O	4.06	4.32	4.70	5.17	4.89	4.70	4.47	4.45	4.55	4.62	4.28	4.56
P ₂ O ₅	0.09	0.10	0.02	0.02	0.02	0.02	0.01	0.01	0.01	0.02	0.06	0.06
LOI	0.45	0.44	0.91	1.09	0.89	0.98	0.50	0.56	0.73	1.05	0.44	0.42
TOTAL	99.70	99.67	99.88	99.90	99.93	99.80	99.84	99.90	99.91	99.84	99.85	99.85
Fe ₂ O ₃ ^t	2.39	2.54	1.82	1.59	1.38	1.70	1.24	1.36	1.24	1.39	1.63	1.49
FeO ^t	2.15	2.29	1.64	1.43	1.24	1.53	1.12	1.22	1.12	1.25	1.47	1.34
FeO ^t / (FeO ^t +MgO)	0.88	0.87	0.95	0.94	0.93	0.95	0.94	0.94	0.93	0.92	0.88	0.87
A/CNK	1.07	1.14	1.05	1.06	0.99	1.00	1.03	1.00	0.99	1.06	1.10	1.13
A/NK	1.30	1.40	1.09	1.11	1.10	1.09	1.11	1.07	1.08	1.12	1.23	1.26
K ₂ O+Na ₂ O	7.74	8.14	8.88	9.04	8.99	8.73	8.32	8.52	8.48	8.59	8.15	8.40
K ₂ O/Na ₂ O	1.10	1.13	1.12	1.34	1.19	1.17	1.16	1.09	1.16	1.16	1.11	1.18
AKI	0.77	0.72	0.92	0.90	0.91	0.92	0.90	0.93	0.93	0.90	0.82	0.79
AR	3.19	2.90	4.99	4.98	4.61	4.78	4.72	4.98	4.83	4.72	3.69	3.57
DI	90.65	89.07	97.11	97.06	95.49	96.23	96.32	96.54	96.07	96.89	94.13	93.84
Li	35.4	34.6	15.0	16.9	11.1	11.0	15.1	9.72	12.4	16.6	35.0	32.2
Be	4.88	5.00	4.96	4.38	4.93	4.40	5.61	4.50	5.15	4.44	7.79	8.06
Sc	7.21	7.87	4.80	3.92	4.78	4.60	4.30	1.52	1.41	1.82	8.12	7.00
V	12.8	16.9	4.69	3.89	5.06	2.92	2.10	2.41	1.62	3.71	5.97	4.94
Cr	3.70	3.92	2.89	2.74	0.76	1.24	0.97	1.32	2.34	1.66	2.83	2.97
Co	2.20	2.54	0.86	0.67	0.58	0.31	0.46	0.33	0.39	0.57	1.02	0.88
Ni	1.23	1.38	3.16	2.10	2.97	0.83	1.17	1.04	1.32	2.37	1.29	1.21
Cu	6.07	8.18	2.51	3.49	2.39	1.70	1.75	1.31	1.41	1.82	3.90	4.64
Zn	42.7	50.2	81.5	69.9	43.6	29.2	30.9	24.8	24.7	62.3	37.3	32.7
Ga	24.2	25.5	21.9	20.5	22.3	22.9	21.8	20.2	20.9	20.7	27.4	27.0
Rb	322	332	206	229	193	185	173	162	207	230	558	539
Sr	115	151	12.6	11.8	20.7	21.9	15.0	14.7	11.6	22.1	24.5	22.0

附表3

测试项目	HTW1605-1a	HTW1605-1b	CXWC62-1a	CXWC62-1b	CXWC63-1	CXWC65-1	CXWG67-1a	CXWC67-1b	CXWC69-1	CXWC69-1b	HTW1610-1a	HTW1610-1b
Y	19.6	22.9	37.8	31.7	49.2	45.4	34.6	33.7	37.6	30.4	21.9	18.7
Mo	1.15	1.34	1.00	0.77	0.54	1.68	1.09	1.01	0.70	0.80	0.22	0.16
Cd	0.10	0.08	0.09	0.10	0.15	0.14	0.03	0.07	0.07	0.26	0.13	0.12
In	0.05	0.07	0.09	0.07	0.19	0.14	0.03	0.04	0.02	0.03	0.04	0.03
Cs	7.26	7.98	2.96	3.60	4.87	3.66	2.75	2.21	2.34	4.30	17.9	16.1
Ba	245	520	56.3	94.7	78.3	60.4	54.6	65.8	40.0	91.1	116	105
La	25.7	29.4	24.4	10.8	33.6	57.0	39.6	36.4	31.6	30.7	14.4	13.7
Ce	—	—	83.1	84.4	98.3	115	89.1	81.9	68.4	72.8	—	—
Pr	5.96	6.94	7.19	3.15	9.00	15.30	10.30	10.60	8.36	8.16	3.93	3.50
Nd	20.8	24.4	29.0	11.9	33.6	56.8	43.2	34.9	31.1	30.1	13.6	12.0
Sm	3.91	4.67	6.10	2.85	7.68	10.10	8.12	6.50	5.70	5.73	2.88	2.36
Eu	0.63	0.82	0.05	0.05	0.10	0.07	0.14	0.13	0.11	0.20	0.22	0.19
Gd	5.19	6.21	5.74	3.27	7.40	9.34	6.25	5.47	5.53	4.90	3.64	3.17
Tb	0.74	0.89	1.15	0.81	1.52	1.57	1.14	0.92	0.96	0.88	0.60	0.49
Dy	3.70	4.40	7.25	5.35	9.04	8.81	5.83	5.38	5.23	5.40	3.33	2.70
Ho	0.69	0.82	1.38	1.13	1.73	1.54	1.19	1.04	1.01	1.00	0.66	0.54
Er	—	2.49	4.10	3.60	5.00	4.44	3.36	3.10	2.89	3.09	2.19	1.82
Tm	0.31	0.35	0.72	0.58	0.79	0.66	0.60	0.47	0.49	0.52	0.36	0.30
Yb	2.16	2.45	4.75	3.77	5.51	4.45	3.67	3.45	3.60	3.48	2.85	2.41
Lu	0.33	0.38	0.69	0.60	0.81	0.65	0.54	0.55	0.54	0.53	0.45	0.39
W	4.02	1.80	2.95	5.78	1.39	5.31	1.20	0.84	5.09	5.08	0.68	0.56
Tl	1.02	1.03	0.85	0.96	0.67	0.83	0.90	0.72	0.85	1.02	1.48	1.42
Pb	11.0	12.6	81.3	42.9	16.7	10.1	14.1	14.7	17.4	20.1	18.3	16.7
Bi	0.51	0.07	0.10	0.09	0.05	0.10	0.28	0.25	0.25	0.04	0.09	0.11
Th	18.3	15.2	30.6	29.1	35.4	40.5	30.1	37.0	42.4	29.2	18.4	15.3
U	6.21	5.00	3.96	2.68	3.16	6.31	3.43	4.95	5.23	3.78	4.40	3.56
Nb	9.00	10.0	18.3	17.5	21.4	16.6	12.4	14.2	19.2	14.3	17.3	16.2
Ta	1.10	1.27	1.52	1.48	1.56	1.58	1.74	1.54	2.23	1.29	3.54	3.68
Zr	251	280	87.0	110	171	142	92.8	107	114	79.9	137	127
Hf	6.67	7.34	4.88	5.85	8.17	6.45	6.51	5.13	6.35	3.88	7.52	7.36
ΣREE	—	—	175.62	132.26	214.07	285.73	213.04	190.81	165.51	167.49	—	—
$\delta^{143}\text{Eu}$	0.43	0.46	0.03	0.05	0.04	0.02	0.06	0.06	0.06	0.11	0.21	0.21
Rb/Sr	2.79	2.20	16.35	19.41	9.32	8.45	11.53	11.02	17.84	10.41	22.75	24.53
Rb/Ba	1.32	0.64	3.66	2.42	2.46	3.06	3.17	2.46	5.18	2.52	4.82	5.11
Nb/Ta	8.19	7.91	12.04	11.82	13.72	10.51	7.13	9.22	8.61	11.09	4.89	4.41
Zr/Hf	37.63	38.20	17.83	18.80	20.93	22.02	14.25	20.86	17.95	20.59	18.16	17.28
(La/Yb) _N	8.55	8.62	3.68	2.05	4.37	9.19	7.74	7.57	6.30	6.33	3.63	4.08
(La/Sm) _N	6.57	6.29	4.00	3.79	4.38	5.64	4.88	5.60	5.54	5.36	4.99	5.81
(Gd/Yb) _N	2.41	2.54	1.21	0.87	1.34	2.10	1.70	1.59	1.54	1.41	1.28	1.31
10000Ca/Al	3.37	3.14	3.17	2.91	3.18	3.38	3.33	3.09	3.21	3.03	3.84	3.59

注：“—”为测试系统误差相关数据。

表4 五十家子岩体锆石Hf同位素组成

Table 4 Zircon Hf isotopic composition of the Wushijiazi pluton

测点号	年龄/Ma	$^{176}\text{Yb}/^{177}\text{Hf}$	$^{176}\text{Lu}/^{177}\text{Hf}$	$^{176}\text{Hf}/^{177}\text{Hf}$	1σ	$^{176}\text{Hf}/^{177}\text{Hf}_\text{i}$	$\epsilon_{\text{Hf}}(t)$	t_{DM1}/Ma	t_{DM2}/Ma	$f_{\text{Lu/Hf}}$
CXWG67-1a-1	145.9	0.100090	0.002379	0.283091	0.000029	0.283084	14.3	236	285	-0.93
CXWG67-1a-2	145.9	0.047273	0.001238	0.282897	0.000022	0.282894	7.5	506	718	-0.96
CXWG67-1a-3	145.9	0.060477	0.001562	0.282969	0.000020	0.282965	10.0	407	557	-0.95
CXWG67-1a-4	145.9	0.048304	0.001290	0.282966	0.000025	0.282962	9.9	409	563	-0.96
CXWG67-1a-5	145.9	0.052258	0.001334	0.282957	0.000021	0.282954	9.6	421	582	-0.96
CXWG67-1a-6	145.9	0.060731	0.001560	0.282987	0.000025	0.282982	10.6	381	517	-0.95
CXWG67-1a-7	145.9	0.048434	0.001279	0.282996	0.000018	0.282992	11.0	366	495	-0.96
CXWG67-1a-8	145.9	0.059733	0.001553	0.282902	0.000022	0.282897	7.6	504	710	-0.95
CXWG67-1a-9	145.9	0.040391	0.001058	0.282901	0.000018	0.282898	7.7	499	709	-0.97

于0.282897~0.283091, $\epsilon_{\text{Hf}}(t)$ 值为7.5~14.3。一阶段模式年龄(t_{DM1})为236~506 Ma,二阶段模式年龄(t_{DM2})为285~718 Ma。

6 讨论

6.1 岩体成因与源区特征

花岗岩成因是地质学界经久不衰的议题,其研究重点在于探讨花岗质岩浆的起源和演化过程。对于花岗岩成因类型的划分,目前最为普遍接受的是I型、S型、M型和A型的分类方案,其中又以I型、S型和A型为常见花岗岩成因类型。上述3类花岗岩的判别,除角闪石、堇青石和碱性暗色矿物等标志性矿物证据外,地球化学图解也被广泛应用。然而,对于高度分异演化的花岗岩,其矿物组成和化学成分都趋近于低共结花岗岩,从而使得上述3类花岗岩的鉴定十分困难(吴福元等,2007),因此其需要多方面证据的综合判定。

近年来对于广泛分布于大兴安岭地区中生代花岗岩的研究发现,绝大多数为A型花岗岩,少数为I型(陈志广等,2008)。五十家子岩体具有富硅(SiO_2 平均值74.89%)、富碱($\text{K}_2\text{O}+\text{Na}_2\text{O}$ 平均值8.50%)、较高的 $\text{FeO}^\text{T}/(\text{MgO}+\text{FeO}^\text{T})$ 值(平均值0.92)、10000Ga/Al值(平均值3.27%)以及较低的MgO(平均值0.14%),CaO(平均值0.64%)和 TiO_2 (平均值0.13%)含量(表3)。微量元素和稀土元素以明显的负Eu异常,富集高场强元素(如Zr、Hf)和大离子亲石元素(如Rb),而亏损Ba、Sr元素为特征。这些特征均与A型花岗岩特征一致(Whalen et al., 1987; Frost and Frost, 2011)。与S型花岗岩相比,五十家子岩体以准铝质—弱过铝质、A/CNK平均值为1.05显著区

别于高硅S型花岗岩强过铝质、A/CNK大于1.1的特征(Clemens et al., 2011)。并且 P_2O_5 与 SiO_2 显示出明显的负相关性(表3),与高硅S型花岗岩成相反趋势(Wu et al., 2003)。而与具有相似高硅特征的高分异I型花岗岩相比,五十家子岩体中Zr元素含量的演化趋势明显与高分异的I型花岗岩不同(图9b)。在一系列判别图解中,五十家子岩体样品点均落在A型花岗岩区域(图9a~d)。综合以上岩石学和地球化学特征推断,五十家子岩体为A型花岗岩。

五十家子岩体在主、微量元素组成上总体具有高硅、富碱,贫钙、镁,富不相容元素Rb而显著亏损Sr、Eu、P、Ti等元素的特征,与大兴安岭南段发生充分结晶分异作用的磨盘山、白音查干和黄岗等岩体相似(周振华等,2010; 管育春等,2017; 姚磊等,2017),且岩体中各岩相分异指数均大于89,指示该岩体为岩浆持续分异演化,镁铁质矿物不断结晶分离(万乐等,2016),而硅、碱、不相容元素残余富集的最终产物。此外,野外可见五十家子岩体中发育有含萤石(电气石)花岗岩、花岗伟晶岩、花岗细晶岩及晶洞构造,反映该岩体由分异演化晚期的富挥发分岩浆固结而成(邱检生等,2008; Dill, 2015)。Sr、Eu、P以及Ti等元素的亏损暗示可能存在斜长石、磷灰石以及钛铁矿的岩浆源区残留或发生了显著的分离结晶作用,而Nb的相对亏损则可能暗示了其源区组成中有地壳物质参与(王永磊等,2012)。Zr-Hf、Nb-Ta等元素由于其一致的地球化学行为而被称为双胞胎元素,在一般岩浆体系中Zr/Hf、Nb/Ta的数值一般无明显变化(Bau, 1996),但当岩浆由于分异而发生性质上的明显改变时,这些比值都将显著变小(Linnen and Keppler, 2002; 吴福元等,2017)。五十

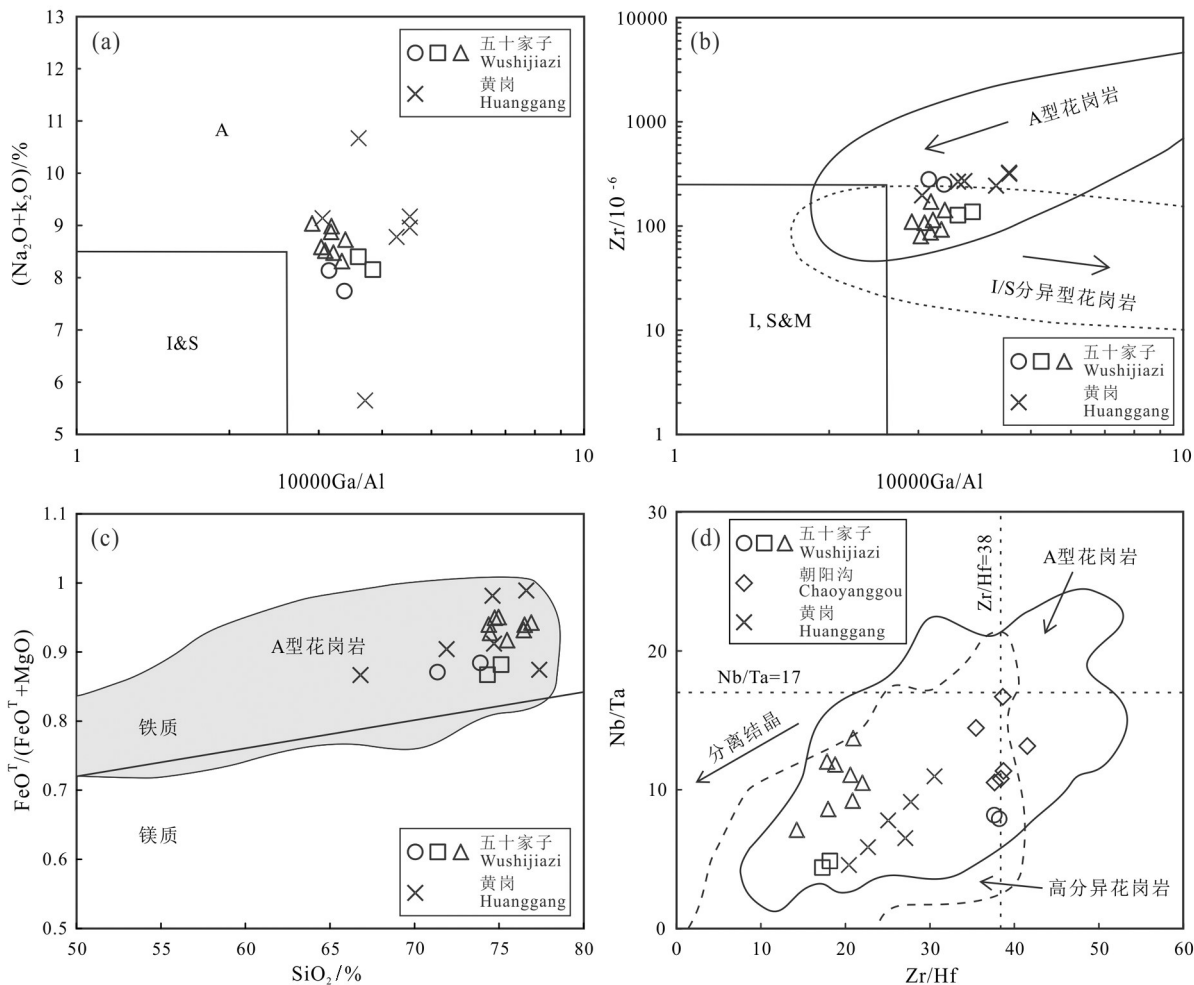


图9五十家子岩体的成因类型判别图解

a, b—I、S、M 和 A 分别表示 I型、S型、M型和 A型花岗岩; a, b, 据 Whalen et al., 1987; c 据 Frost and Frost, 2011; b 和 d 中实线和虚线部分据吴福元等(2017); 黄岗数据引自周振华等(2010); 朝阳沟数据归于本文二长花岗岩相带, 引自万乐等(2016)

Fig.9 Chemical discrimination diagrams for the Wushijiazi pluton

a, b—I, S, M and A represent I-, S-, M- and A-type granites respectively; a, b, after Whalen et al., 1987; c after Frost and Frost, 2011; the solid line and dotted line field in figure b and d is from Wu et al.(2017); Huanggang data is after Zhou et al.(2010); Chaoyanggou data is attributed to the monzonite facies in this paper and is from Wan et al.(2016)

家子岩体各相带演化序列(从早到晚:含黑云母二长花岗岩相—含黑云母正长花岗岩相—斑状黑云母正长花岗岩相)与其岩石 Zr/Hf 、 Nb/Ta 比值逐渐降低的趋势一致(图 9d), 这也表明五十家子岩体经历了显著地分离结晶作用, 且晚阶段侵位的斑状含黑云母正长花岗岩和斑状黑云母正长花岗岩结晶分异程度更高。综合以上特征, 笔者认为五十家子岩体形成过程中经历了充分的分异演化。

五十家子岩体的 Nb/Ta 比值为 $4.41\sim 13.72$, 平均值为 9.13 , 远低于幔源岩浆 $\text{Nb}/\text{Ta}=17.5\pm 2$ 的比值, 而与壳源岩浆的 Nb/Ta 比值($11\sim 12$)相近(管琪等,

2010); Zr/Hf 比值介于 $14.25\sim 38.20$, 平均值为 22.04 , 同样远低于地幔的 Zr/Hf 比值($34\sim 60$), 而接近于地壳平均值(35.5) (Wedepohl, 1994), 表明源区物质可能来源于地壳的部分熔融。五十家子斑状含黑云母正长花岗岩中锆石样品的 $\epsilon_{\text{Hf}}(t)$ 全部为正值($+7.5\sim +14.3$), 并有年轻的二阶段模式年龄($t_{\text{DM2}}=285\sim 718$ Ma), 在 $\epsilon_{\text{Hf}}(t)-t$ 图解中(图 10), 样品点全部落入球粒陨石和亏损地幔之间的兴蒙造山带内, 而据 Zeng et al.(2016)分析数据显示五十家子二长花岗岩的 $\epsilon_{\text{Hf}}(t)$ 分布于 $+6.3\sim +9.0$, 同样拥有年轻的二阶段模式年龄($t_{\text{DM2}}=627\sim 800$ Ma)。同时在 Sr 、 Nd 、 Pb

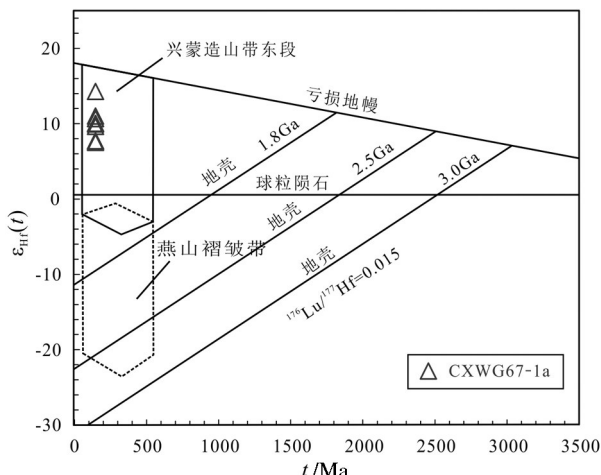


图10 五十家子斑状含黑云母正长花岗岩中锆石的 $\varepsilon_{\text{Hf}}(t)$ - t 图解
(兴蒙造山带东段兴蒙造山带及燕山褶皱带数据引自Yang et al., 2006)

Fig.10 $\varepsilon_{\text{Hf}}(t)$ - t diagram of the Wushijiazi porphyritic biotite-bearing syenogranite

(The eastern section of Mongol—Hinggan Orogenic Belt and Yanshan Fold Belt data is from Yang et al., 2006)

同位素组成上,五十家子岩体中斑状含黑云母正长花岗岩和含黑云母二长花岗岩具有正的 $\varepsilon_{\text{Nd}}(t)$ 值(+1.3~+2.1和+1.1~+2.0, Ding et al., 2016)、低 $^{87}\text{Sr}/^{86}\text{Sr}$ 比值(0.70418~0.70952和0.70293~0.71305, Ding et al., 2016)和年轻的Nd模式年龄(795~1020 Ma和866~1121 Ma, Ding et al., 2016),与大兴安岭南段许多中生代花岗岩的Sr,Nd同位素值相似,反映了其源区中年轻物质的贡献占主导地位(Wu et al., 2002; 李竟妍等, 2014),这与五十家子岩体Hf同位素反映的结果一致,因此笔者认为五十家子花岗岩体的源区物质主要来自年轻下地壳的部分熔融。前人研究认为该区大量壳幔过渡带残留的古生代洋壳在中生代底侵背景下与下地壳的物质一起部分熔融,形成了壳幔混熔岩浆(邵济安等, 2010),而壳源型花岗岩的 $^{207}\text{Pb}/^{204}\text{Pb}$ 通常大于15.600,壳幔混熔型花岗岩的 $^{207}\text{Pb}/^{204}\text{Pb}$ 通常低于15.600(周振华等, 2010),五十家子岩体中斑状含黑云母正长花岗岩和含黑云母二长花岗岩的 $^{207}\text{Pb}/^{204}\text{Pb}$ 比值分别为15.551~15.572和15.564~15.596(Ding et al., 2016),显示壳幔混熔特征。五十家子斑状含黑云母二长花岗岩中发育大量暗色微粒包体,可能暗示该岩体形

成过程中有幔源物质参与,尽管暗色微粒包体亦可能属于堆晶成因。虽未能获得斑状黑云母正长花岗岩的同位素数据,但考虑到五十家子各岩相地球化学特征的相似性及时空演化关系,同时结合区域地质背景,笔者推断五十家子各岩相的源区很大可能是相同的。综上所述,研究区花岗岩岩浆的源区物质主要来源于年轻下地壳的部分熔融,并可能经历了与幔源岩浆的混合过程形成了壳幔混源岩浆,壳幔混源岩浆形成后又经高程度分异演化并于浅部先后侵位,最终固结形成了五十家子花岗岩体。

6.2 构造背景

A型花岗岩最早定义为碱性、贫水和非造山的花岗质岩石(Loiselle and Wones, 1979),后来研究发现A型花岗岩也可以形成于造山后环境(Eby, 1992; 吴福元等, 2007)。通常认为A型花岗岩的形成主要与伸展构造体制有关(Whalen et al., 1987; Eby, 1992; Wu et al., 2002; Li et al., 2007; 贾小辉等, 2009),是构造环境判别的重要岩石学标志(吴福元等, 2007; 贾小辉等, 2009)。五十家子岩体形成于晚侏罗世—早白垩世,属A型花岗岩,总体表现为张性花岗岩特征,与该时期区域上的岩石圈伸展环境(邵济安等, 1998, 2001a,b, 2002; 郭锋等, 2001; Wu et al., 2002; 王京彬等, 2002; 林强等, 2003; Meng, 2003; Liu et al., 2005; Zhang et al., 2006; 张玉涛等, 2006; Yang et al., 2007; Donskaya et al., 2008; Wang et al., 2011; Zeng et al., 2015; Fu et al., 2016; Wan et al., 2019)相对应。在Rb-(Y+Nb)构造环境判别图解中,五十家子岩体大多落入后碰撞花岗岩区域(图11),而由于斑状黑云母正长花岗岩在五十家子岩体中分异程度最高,其强烈富集不相容元素Rb的特征,可能是导致其落入了后碰撞花岗岩区域上方的原因,构造环境判别图解进一步揭示了晚侏罗世—早白垩世期间研究区处于造山期后伸展的大地构造背景中。

大兴安岭南段地区在中生代发生了强烈的构造—岩浆活动,并引发了成矿大爆发(周振华等, 2010; 翟德高等, 2012)。然而,对于区域上中生代晚期大规模成岩成矿事件的构造背景受何种体制制约尚有争议。前人提出的几种主流观点如前文所述。近期大量研究成果趋于表明华北板块与西伯利亚板块最终缝合时间为晚二叠世—早中三叠世

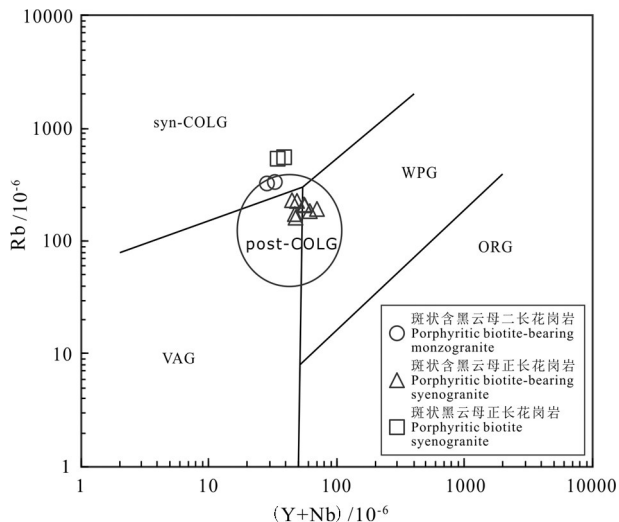


图11 五十家子岩体(Y+Nb)-Rb构造环境判别图解(据 Pearce, 1996)

ORG—大洋中脊花岗岩; WPG—板内花岗岩; VAG—火山弧花岗岩; Syn-COLG—同碰撞花岗岩

Fig.11 (Y+Nb)-Rb diagram indicating possible tectonic settings for the Wushijiazi pluton (after Pearce, 1996)
ORG—Ocean Ridge Granites; WPG—Intraplate Granites; VAG—Volcanic Arc Granites; Syn-COLG—Synchronous-Collision Granites

(Davis et al., 2004; Li et al., 2006; Xiao et al., 2009; 韩国卿等, 2011; Xu et al., 2013; 刘锐等, 2016), 其造山后环境持续到晚中生代的可能性较小(杨奇荻等, 2014)。三叠纪—晚侏罗世, 蒙古—鄂霍茨克洋自西向东呈剪刀式逐渐闭合(Zonenshain et al., 1990; 莫申国等, 2005), 而大兴安岭南段地区的侵入岩及火山岩年龄也表现出自西向东逐渐变年轻的趋势(Meng, 2003; Wang et al., 2006), 已有研究显示蒙古—鄂霍茨克构造体系对兴安板块的影响一直持续到早白垩世早期(Tang et al., 2015; Li et al., 2017), 并在晚中生代完成了碰撞挤压到碰撞后伸展体质的转换(Meng, 2003), 因此时空关系方面显示蒙古—鄂霍茨克构造体系对研究区的构造—岩浆活动具有显著影响。另外, 大量研究表明, 中国东部从晚侏罗世至白垩纪受到古太平洋板块的西向俯冲(Zhou et al., 2006; Li and Li, 2007; Sun et al., 2007; Zhang et al., 2010; Shu et al., 2016; 朱日祥等, 2019), 其俯冲作用影响距离可达 1300 km(Li and Li, 2007), 并且由于古太平洋板块俯冲方向的改变, 使得区域构造格局完成了从挤压到伸展的转换过程(Zhang et al., 2010)。前述构造体制的转变导致了岩

石圈的拆沉减薄和软流圈的上涌, 随后引发了大兴安岭地区晚中生代剧烈的岩浆活动, 不仅形成了区域上广泛分布的A型花岗岩(Wu et al., 2002; Zeng et al., 2015; Wan et al., 2019; 本文), 还形成了区内大量与晚中生代高度分异演化的钙碱性—碱性侵入体有关的稀有、稀土多金属矿床(如白音查干、黄岗梁、哈什吐、巴尔哲)。这与前人统计分析得出的中国东部在中生代时期发生了成矿动力学背景的构造体质大转折以及大规模成岩成矿作用等结论一致(毛景文等, 2003, 2005)。除上述特征外, 前人对区内发现的双峰式火山岩(郭锋等, 2001; 林强等, 2003; Zhang et al., 2006)、变质核杂岩(Liu et al., 2005; Yang et al., 2007; Donskaya et al., 2008; Wang et al., 2011; Fu et al., 2016)、同时代双峰式镁铁质和长英质岩墙群(邵济安等, 1998, 2001a, b, 2002; 张玉涛等, 2006)及伸展性盆地(Meng, 2003)的相关研究也证实了区域上晚中生代的岩石圈伸展减薄背景。综上所述, 五十家子岩体形成于晚侏罗世—早白垩世早期, 属于造山后向非造山环境的转折阶段, 总体表现为具有张性花岗岩的特征, 反映了晚中生代研究区岩浆演化的伸展构造背景。

这种活跃的伸展背景可能受蒙古—鄂霍茨克构造体系和古太平洋构造体系的双重制约。结合区域地质背景及前人研究成果, 笔者认为五十家子岩体形成于岩石圈伸展减薄及软流圈上涌的构造背景下。

6.3 地质意义

五十家子花岗岩体形成于中生代晚期, 这一时期研究区为造山期后伸展背景, 且区域深大断裂构造和岩浆作用发育, 对锡多金属成矿极为有利(陈郑辉等, 2015)。同时, 年代学数据和地球化学数据分别显示该岩体中各岩相侵位时代相距不远, 且地球化学特征相似, 因此笔者认为该岩体为晚侏罗世—早白垩世3个阶段侵入的杂岩体。而杂岩体代表深部岩浆分异、演化最充分最彻底的一类岩体, 因而也是最有可能成为成矿岩体的一类岩体组合(刘家远, 2003)。

毛景文等(2005)的研究表明, 140 Ma左右为大兴安岭南段地区锡多金属成矿高峰期, 同时, 这一时期是花岗岩侵位的高峰期, 经高度分异演化并于浅部侵位的花岗质岩浆是引发区内爆发式成矿的

关键因素。马星华等(2009)也提出,西拉木伦河断裂与大兴安岭主脊断裂交汇处众多金属矿床成矿高峰期处于250~220 Ma及150~130 Ma两期,其中以150~130 Ma这一期成矿事件最为显著。五十家子岩体形成于晚侏罗世—早白垩世,其成岩时代与区域成矿时代基本一致,区域上隶属于前人划分的黄岗梁—甘珠尔庙晚中生代Sn-Cu多金属成矿带(Ouyang et al., 2015)。

花岗质岩浆的强烈结晶分异促使残留相富集不相容元素及挥发分(如Sn、W、Li、Be、Cs、F、B)(Romer and Kroner, 2016),与锡多金属成矿相关的花岗岩通常具有高度分异演化的特征(祝新友等,2012;吴福元等,2017),并且大多数锡多金属矿床的形成与伸展背景下地幔物质的上涌有关(Kontak and Clark, 2002)。五十家子岩体中晶洞构造发育,且伴生含萤石花岗岩、含电气石花岗岩、花岗伟晶岩及花岗细晶岩,表明岩浆分异晚期富含挥发分的特点,是岩浆体系进入到高演化阶段的岩石学证据(Bakker and Elburg, 2006; Dill, 2015),结合前文主、微量元素分析结果,可知五十家子岩体在岩相学和地球化学上均显示具有高程度分异演化特征。在Zr/Hf-Nb/Ta图解中五十家子岩体样品点几乎全落于高度分异结晶区域内(图9d),且相对早阶段斑状含黑云母二长花岗岩,斑状含黑云母正长花岗岩和斑状黑云母正长花岗岩结晶分异程度更高。五十家子花岗岩体属伸展背景下形成的A型花岗岩,侵位于大兴安岭南段晚侏罗世—早白垩世构造—岩浆活动的鼎盛期(王京彬等,2002),其成岩过程具有壳幔混源、高度分异演化及深源浅侵位等特征,为成矿元素的运移、富集和保存提供了良好条件,并与区域上典型锡多金属成矿相关花岗岩体(如维拉斯托、白音查干和黄岗岩体)的地质地球化学特征有许多相似之处(周振华等,2010;祝新友等,2016;姚磊等,2017),是锡多金属成矿的有利地质体。

五十家子岩体是大兴安岭南段一个重要的含矿岩体,岩体中分布有多处矿床(点)和物化探异常点,如宝盖沟锡矿、新林镇猪家岭钼铁铜矿、哈什吐钼矿床、五十家子铅锌银矿以及小海清铁钨锡矿等^①。岩体中矿化异常具有规律性,矿化多发育在岩体内不同岩相或岩体与二叠纪地层的接触部位(图1),且构造控矿作用显著。因此,岩体内部不同

岩相及岩体与围岩地层的接触部位具有重要的找矿潜力。

7 结 论

(1)本次研究通过LA-ICP-MS锆石U-Pb同位素测年方法测得五十家子岩体中斑状含黑云母二长花岗岩、斑状含黑云母正长花岗岩、斑状黑云母正长花岗岩年龄分别是(150.3±1.3) Ma,(145.9±1.8) Ma,(137.1±2.2) Ma,可知该岩体为晚侏罗世—早白垩世的产物。

(2)岩石地球化学分析结果显示五十家子花岗岩岩体总体具有高硅、富碱、低铝,贫钙、镁、铁,富Rb而显著亏损Sr、Eu、P、Ti等元素的特征,属碱性、准铝质-弱过铝质A型花岗岩;锆石Hf同位素研究结果显示,五十家子花岗岩体源区主要为年轻下地壳,并可能有幔源岩浆的参与。

(3)五十家子花岗岩体形成于造山后向非造山环境转变的伸展背景下,该背景可能受蒙古—鄂霍茨克构造体系和古太平洋构造体系的双重制约。

(4)该岩体成岩时代与区域上锡多金属成矿时代一致,并具有对成矿有利的高分异特征和构造背景,结合区域物化探异常分布特征综合研究显示其可能为锡多金属成矿的有利地质体。

致谢:野外地质工作期间得到了北京矿产地质研究院管育春、蒋斌斌等工程师的大力支持和帮助;室内研究及论文撰写过程中均得到了北京矿产地质研究院杨尚松博士的热情帮助和指导;实验工作得到了合肥工业大学资源与环境工程学院汪方跃老师的详细指导;审稿专家对论文提出了建设性的修改意见,使论文更加完善。在此一并致以由衷的感谢!

注释

① 北京矿产地质研究院. 2017. 内蒙古赤峰有色金属基地综合地质调查2017年度进展报告[R].

References

- Albarède F, Scherer E E, Blichert-Toft J, Rosing M, Simionovici A, Bizzarro M. 2006. γ -ray irradiation in the early Solar System and the conundrum of the ^{176}Lu decay constant[J]. *Geochimica et Cosmochimica Acta*, 70(5): 1261–1270.
- Andersen T. 2002. Correction of common lead in U-Pb analyses that

- do not report ^{204}Pb [J]. *Chemical Geology*, 192(1): 59–79.
- Bakker R J, Elburg M A. 2006. A magmatic–hydrothermal transition in Arkaroola (northern Flinders Ranges, South Australia): From diopside– titanite pegmatites to hematite– quartz growth[J]. *Contributions to Mineralogy & Petrology*, 152(5): 541–569.
- Bau M. 1996. Controls on the fractionation of isovalent trace elements in magmatic and aqueous systems: Evidence from Y/Ho, Zr/Hf, and lanthanide tetrad effect[J]. *Contributions to Mineralogy & Petrology*, 123(3): 323–333.
- Blicherttoft J, Albarède F. 1997. The Lu–Hf isotope geochemistry of chondrites and the evolution of the mantle–crust system[J]. *Earth & Planetary Science Letters*, 148(1/2): 243–258.
- Chen Jianlin, Guo Yuansheng, Fu Shanming. 2004. Research progress of ISMA granite classification review[J]. *Journal of Gansu Geology*, 13(1): 67–73(in Chinese with English abstract).
- Chen Zhenghui, Wang Denghong, Sheng Jifu, Ying Lijuan, Liang Ting, Wang Chenghui, Liu Lijun, Wang Yonglei. 2015. The metallogenetic regularity of tin deposits in China[J]. *Acta Geologica Sinica*, 89(6): 1038–1050(in Chinese with English abstract).
- Chen Zhiguang, Zhang Lianchang, Wu Huaying, Wan Bo, Zeng Qingdong. 2008. Geochemistry study and tectonic background of A style host granite in Nianzizou molybdenum deposit in Xilamulun molybdenum metallogenic belt, Inner Mongolia[J]. *Acta Petrologica Sinica*, 24(4): 879–889(in Chinese with English abstract).
- Clemens J D, Stevens G, Farina F. 2011. The enigmatic sources of I-type granites: The peritectic connexion[J]. *Lithos*, 126(3): 174–181.
- Davis G A, Xu Bei, Zheng Yadong, Zhang Weijie. 2004. Indosinian extension in the Solonker suture zone: The Sonid Zuogui metamorphic core complex, Inner Mongolia, China[J]. *Earth Science Frontiers*, 11(3): 135–144.
- Dill H G. 2015. Pegmatites and aplites: Their genetic and applied ore geology[J]. *Ore Geology Reviews*, 69: 417–561.
- Ding Chengwu, Dai Pan, Bagas Leon, Nie Fengjun, Jiang Sihong, Wei Junhao, Ding Chengzhen, Zuo Pengfei, Zhang Ke. 2016. Geochemistry and Sr–Nd–Pb isotopes of the granites from the Hashitu Mo Deposit of Inner Mongolia, China: Constraints on their origin and tectonic setting[J]. *Acta Geologica Sinica*, 90(1): 106–120.
- Donskaya T V, Windley B F, Mazukabzov A M, Kröner A, Sklyarov E V, Gladkochub D P, Ponomarchuk V A, Badarch G, Reichow M K, Hegner E. 2008. Age and evolution of late Mesozoic metamorphic core complexes in southern Siberia and northern Mongolia[J]. *Journal of the Geological Society*, 165(1): 405–421.
- Eby G N. 1992. Chemical subdivision of the A–type granitoids: Petrogenetic and tectonic implications[J]. *Geology*, 20(7): 641–644.
- Fan Weiming, Guo Feng, Wang Yuejun, Ge Lin. 2003. Late Mesozoic calc–alkaline volcanism of post–orogenic extension in the northern Da Hinggan Mountains, northeastern China[J]. *Journal of Volcanology and Geothermal Research*, 121(1): 115–135.
- Frost C D, Frost B R. 2011. On Ferroan (A–type) granitoids: Their compositional variability and modes of origin[J]. *Journal of Petrology*, 52(1): 39–53.
- Fu Lebing, Wei Junhao, Tan Jun, Santosh M, Zhang Daohan, Chen Jiajie, Li Yanjun, Zhao Shaoqing, Peng Lina. 2016. Magma mixing in the Kalaqin core complex, northern North China Craton: Linking deep lithospheric destruction and shallow extension[J]. *Lithos*, 260: 390–412.
- Griffin W L, Pearson N J, Belousova E A, Jackson S E, Van Achterbergh E, O'Reilly S Y, Shee S R. 2000. The Hf isotope composition of cratonic mantle: LAM–MC–ICPMS analysis of zircon megacrysts in kimberlites[J]. *Geochimica et Cosmochimica Acta*, 64(1): 133–147.
- Guan Qi, Zhu Dicheng, Zhao Zhidan, Zhang Liangliang, Liu Min, Li Xiaowei, Yu Feng, Mo Xuanxue. 2010. Late Cretaceous adakites in the eastern segment of the Gangdese Belt, southern Tibet: Products of Neo–Tethyan ridge subduction?[J]. *Acta Petrologica Sinica*, 26(7): 2165–2179(in Chinese with English abstract).
- Guan Yuchun, Yang Zongfeng, Zhu Xinyou, Zou Tao, Cheng Xiyin, Tang Lei, Deng Haihui. 2017. Petrogenesis and geological significance of the Beidashan complex rockmass, Inner Mongolia[J]. *Geotechnical Engineering World*, 8(6): 1054–1068(in Chinese with English abstract).
- Guo Feng, Fan Weiming, Wang Yuejun, Lin Ge. 2001. Petrogenesis of the late Mesozoic bimodal volcanic rocks in the southern Da Hinggan Mts, China[J]. *Acta Petrologica Sinica*, 17(1): 161–168(in Chinese with English abstract).
- Han Guoqing, Liu Yongjiang, Wen Quanbo, Li Wei, Wu Linna, Zhao Yingli, Ding Ling, Zhao Limin, Liang Chenyue. 2011. LA–ICP–MS U–Pb dating of detrital zircons from the Permian sandstones in north side of Xar Moron River suture belt and its tectonic implications[J]. *Earth Science—Journal of China University of Geosciences*, 36(4): 687–702(in Chinese with English abstract).
- Hofmann A W. 1988. Chemical differentiation of the Earth: The relationship between mantle, continental crust, and oceanic crust[J]. *Earth & Planetary Science Letters*, 90(3): 297–314.
- Jia Xiaohui, Wang Qiang, Tang gongjian. 2009. A–type granites: Research progress and implications[J]. *Geotectonica et Metallogenia*, 33(3): 465–480(in Chinese with English abstract).
- Kontak D J, Clark A H. 2002. Genesis of the Giant, Bonanza San Rafael Lode Tin Deposit, Peru: Origin and significance of pervasive alteration[J]. *Economic Geology*, 97(8): 1741–1777.
- Li J Y. 2006. Permian geodynamic setting of Northeast China and adjacent regions: closure of the Paleo–Asian Ocean and subduction of the Paleo–Pacific Plate[J]. *Journal of Asian Earth Sciences*, 26(3): 207–224.
- Li Jingyan, Guo Feng, Li Chaowen, Li Hongxia, Zhao Liang. 2014. Neodymium isotopic variations of Late Paleozoic to Mesozoic I–

- and A-type granitoids in NE China: Implications for tectonic evolution[J]. *Acta Petrologica Sinica*, 30(7): 1995–2008(in Chinese with English abstract).
- Li Xianhua, Li Zhengxiang, Li Wuxian, Liu Ying, Yuan Chao, Wei Gangjian, Qi Changshi. 2007. U-Pb zircon, geochemical and Sr-Nd-Hf isotopic constraints on age and origin of Jurassic I- and A-type granites from central Guangdong, SE China: A major igneous event in response to foundering of a subducted flat-slab?[J]. *Lithos*, 96(1): 186–204.
- Li Yu, Xu Wenliang, Wang Feng, Pei Fuping, Tang Jie, Zhao Shuo. 2017. Triassic volcanism along the eastern margin of the Xing'an Massif, NE China: Constraints on the spatial-temporal extent of the Mongol-Okhotsk tectonic regime[J]. *Gondwana Research*, 48: 205–223.
- Li Zhenzhen, Qin Kezhang, Zhao Junxing, Li Guangming, Su shiqiang. 2019. Basic characteristics, research progresses and prospects of Sn-Ag-base metal metallogenetic system[J]. *Acta Petrologica Sinica*, 35(7): 1979–1998(in Chinese with English abstract).
- Li Zhengxiang, Li Xianhua. 2007. Formation of the 1300-km-wide intracontinental orogen and postorogenic magmatic province in Mesozoic South China: A flat-slab subduction model[J]. *Geology*, 35(2): 179–182.
- Lin Qiang, Ge Wenchun, Cao Lin, Sun Deyou, Lim Kyunggook. 2003. Geochemistry of Mesozoic volcanic rocks in Da Hinggan Ling: The bimodal volcanic rocks[J]. *Geochimica*, 32(3): 208–222(in Chinese with English abstract).
- Lin Qiang, Ge Wenchun, Wu Fuyuan, Sun Deyou, Cao Lin. 2004. Geochemistry of Mesozoic granites in Da Hinggan Ling ranges[J]. *Acta Petrologica Sinica*, 20(3): 403–412(in Chinese with English abstract).
- Linnen R L, Keppler H. 2002. Melt composition control of Zr/Hf fractionation in magmatic processes[J]. *Geochimica et Cosmochimica Acta*, 66(18): 3293–3301.
- Liu Jiayuan. 2003. Compound massif and complex massif—The two basic forms of the massif association of granitoid and their significance[J]. *Contributions to Geology and Mineral Resources Research*, 18(3): 143–148(in Chinese with English abstract).
- Liu Junlai, Davis G A, Lin Zhiyong, Wu Fuyuan. 2005. The Liaonian metamorphic core complex, Southeastern Liaoning Province, North China: A likely contributor to Cretaceous rotation of Eastern Liaoning, Korea and contiguous areas[J]. *Tectonophysics*, 407(1): 65–80.
- Liu Rui, Yang Zhen, Xu Qidong, Zhang Xiaojun, Yao Chunliang. 2016. Zircon U-Pb ages, elemental and Sr-Nd-Pb isotopic geochemistry of the Hercynian granitoids from the southern segment of the Da-Hinggan Mts: Petrogenesis and tectonic implications[J]. *Acta Petrologica Sinica*, 32(5): 1505–1528(in Chinese with English abstract).
- Liu Yongjiang, Li Weiming, Feng Zhiqiang, Wen Quanbo, Neubauer F, Liang Chenyue. 2017. A review of the Paleozoic tectonics in the eastern part of Central Asian Orogenic Belt[J]. *Gondwana Research*, 43: 123–148.
- Loiselle M C, Wones D R. 1979. Characteristics and origin of anorogenic granites[J]. *Abstracts with Programs—Geological Society of America*, 11(7): 468.
- Ludwig K R. 2003. ISOPLOT 3.00: A Geochronological Toolkit for Microsoft Excel[M]. California: Berkeley Geochronology Center Special Publication, 1–70.
- Ma Xinghua, Chen Bin, Lai Yong, Lu Yinghuai. 2009. Petrogenesis and mineralization chronology study on the Aolunhua porphyry Mo deposit, inner Mongolia, and its geological implications[J]. *Acta Petrologica Sinica*, 25(11): 2939–2950(in Chinese with English abstract).
- Maniard P D, Piccoli P M. 1989. Tectonic discrimination of granitoids[J]. 101(5): 635–643.
- Mao Jingwen, Zhang Zuoheng, Yu Jinjie, Wang Yitian, Niu Baogui. 2003. Mesozoic tectonic setting of large scale ore-forming in east China and adjacent areas: Revealed by precise ages of metallic deposits[J]. *Science in China(series D)*, 33(4): 289–299(in Chinese).
- Mao Jingwen, Xie Guiqing, Zhang Zuoheng, Li Xiaofeng, Wang Yitian, Zhang Changqing, Li Yongfeng. 2005. Mesozoic large-scale metallogenetic pulses in North China and corresponding geodynamic settings[J]. *Acta Petrologica Sinica*, 21(1): 169–88(in Chinese with English abstract).
- Mao J W, Xie G Q, Pirajno F, Ye H S, Wang Y B, Li Y F, Xiang J F, Zhao H J. 2010. Late Jurassic–Early Cretaceous granitoid magmatism in Eastern Qinling, central-eastern China: SHRIMP zircon U-Pb ages and tectonic implications[J]. *Journal of the Geological Society of Australia*, 57(1): 51–78.
- Meng Qingren. 2003. What drove late Mesozoic extension of the northern China-Mongolia tract?[J]. *Tectonophysics*, 369(3): 155–174.
- Mo Shenguo, Han Meilian, Li Tiejin. 2005. Composition and orogenic processes of Mongolia-Okhotsk Orogen[J]. *Journal of Shandong University of Science and Technology(Nature Science)*, 24(3): 50–53(in Chinese with English abstract).
- Ouyang Hegen, Mao Jingwen, Zhou Zhenhua, Su Huiming. 2015. Late Mesozoic metallogeny and intracontinental magmatism, southern Great Xing'an Range, northeastern China[J]. *Gondwana Research*, 27(3): 1153–1172.
- Pearce J A. 1996. Sources and settings of granitic rocks[J]. *Episodes*, 19(4): 120–125.
- Petro W L, Vogel T A, Wilband J T. 1979. Major-element chemistry of plutonic rock suites from compressional and extensional plate boundaries[J]. *Chemical Geology*, 26(3/4): 217–235.
- Qiu Jiansheng, Xiao Er, Hu Jian, Xu Xisheng, Jiang Shaoyong, Li

- Zhen. 2008. Petrogenesis of highly fractionated I-type granites in the coastal area of northeastern Fujian Province: Constraints from zircon U-Pb geochronology, geochemistry and Nd-Hf isotopes[J]. *Acta Petrologica Sinica*, 24(11): 2468–2484(in Chinese with English abstract).
- Romer R L, Kröner U. 2016. Phanerozoic tin and tungsten mineralization—Tectonic controls on the distribution of enriched protoliths and heat sources for crustal melting[J]. *Gondwana Research*, 31: 60–95.
- Rudnick R L, Gao S. 2003. Composition of the Continental Crust[M]. Oxford: Elsevier–Pergamon, 1–64.
- Shao Ji'an, Zhang Lüqiao, Mou Baolei. 1998. Thermo-tectonic evolution in middle and south part of Dahinggan[J]. *Science in China (Series D)*, 28(3): 193–200(in Chinese).
- Shao Ji'an, Li Xianhua, Zhang Lüqiao, Mou Baolei, Liu Yulin. 2001a. Geochemical condition for genetic mechanism of the Mesozoic bimodal dike swarms in Nankou–Guyaju[J]. *Geochimica*, 30(6): 517–524(in Chinese with English abstract).
- Shao Ji'an, Liu Futian, Chen Hui, Han Qingjun. 2001b. Relationship between Mesozoic Magmatism and Subduction in Da Hinggan–Yanshan Area[J]. *Acta Geologica Sinica*, 75(1): 56–63(in Chinese with English abstract).
- Shao Ji'an, Zhang Lüqiao. 2002. Mesozoic dyke swarms in the north of Northern China[J]. *Acta Petrologica Sinica*, 18(3): 312–318(in Chinese with English abstract).
- Shao Ji'an, Mu Baolei, Zhu Huizhong, Zhang Lüqiao. 2010. Material source and tectonic settings of the Mesozoic mineralization of the Da Hinggan Mountains[J]. *Acta Petrologica Sinica*, 26(3): 649–656 (in Chinese with English abstract).
- Shi Changyi, Yan Mingcai, Liu Chongmin, Chi Qinghua, Hu Shuqi, Gu Tiexin, Bu Wei, Yan Weidong. 2005. Abundances of chemical elements in granitoids of China and their characteristics[J]. *Geochimica*, 34(5): 470–482(in Chinese with English abstract).
- Shu Qihai, Chang Zhaoshan, Lai Yong, Zhou Yitao, Sun Yi, Yan Cong. 2016. Regional metallogeny of Mo-bearing deposits in Northeastern China, with new Re-Os dates of porphyry Mo deposits in the Northern Xilamulun District[J]. *Economic Geology*, 111(7): 1783–1798.
- Sun S S, McDonough W F. 1989. Chemical and isotopic systematics of oceanic basalts: Implications for mantle composition and processes[J]. *Geological Society London Special Publications*, 42 (1): 313–345.
- Sun Weidong, Ding Xing, Hu Yanhua, Li Xianhua. 2007. The golden transformation of the Cretaceous plate subduction in the west Pacific[J]. *Earth and Planetary Science Letters*, 262(3/4): 533–542.
- Tang Jie, Xu Wenliang, Wang Feng, Zhao Shuo, Li Yu. 2015. Geochronology, geochemistry, and deformation history of Late Jurassic–Early Cretaceous intrusive rocks in the Erguna Massif, NE China: Constraints on the late Mesozoic tectonic evolution of the Mongol–Okhotsk orogenic belt[J]. *Tectonophysics*, 658: 91–110.
- Wakita K, Metcalfe I. 2005. Ocean Plate Stratigraphy in East and Southeast Asia[J]. *Journal of Asian Earth Sciences*, 24(6): 679–702.
- Wan Le, Liu Zhenghong, Li Gang, Xin Houtian. 2016. Zircon U-Pb dating, geochemistry and their significance of the Early Cretaceous Chaoyanggou granites in Linxi, Inner Mongolia[J]. *Geology and Resources*, 25(1): 1–10(in Chinese with English abstract).
- Wan Le, Lu Chengdong, Zeng Zuoxun, Mohammed Adil S, Liu Zhenghong, Dai Qingqin, Chen Kangli. 2019. Nature and significance of the late Mesozoic granitoids in the southern Great Xing'an range, eastern Central Asian Orogenic Belt [J]. *International Geology Review*, 61(5): 584–606.
- Wang Fei, Zhou Xinhua, Zhang Lianchang, Ying Jifeng, Zhang Yutao, Wu Fuyuan, Zhu Rixiang. 2006. Late Mesozoic volcanism in the Great Xing'an Range (NE China): Timing and implications for the dynamic setting of NE Asia[J]. *Earth and Planetary Science Letters*, 251(1): 179–198.
- Wang Jingbin, Wang Yuwang, Wang Lijuan. 2002. Mesozoic extension–metallagenic system in suthern part of Da Hinggan Mountains, China[J]. *Mineral Deposits*, 21(S1): 241–244(in Chinese).
- Wang Pujun, Liu Wanzhu, Wang Shuxue, Song Weiwei. 2002. $^{40}\text{Ar}/^{39}\text{Ar}$ and K/Ar dating on the volcanic rocks in the Songliao basin, NE China: Constraints on stratigraphy and basin dynamics[J]. *International Journal of Earth Sciences*, 91(2): 331–340.
- Wang Tao, Zheng Yadong, Zhang Jinjiang, Zeng Lingsen, Donskaya T, Guo Lei, Li Jianbo. 2011. Pattern and kinematic polarity of late Mesozoic extension in continental NE Asia: Perspectives from metamorphic core complexes[J]. *Tectonics*, 30(6).
- Wang Yang. 2009. Geochemistry of the Baicha A-type granite in Beijing municipality: Petrogenetic and tectonic implications[J]. *Acta Petrologica Sinica*, 25(1): 13–24(in Chinese with English abstract).
- Wang Yonglei, Wang Denghong, Zhang Changqing, Hou Kejun, Wang Chenghui. 2011. LA-ICP-MS zircon U-Pb dating of the Qinjia granite in Guangxi Province and its geologic significance[J]. *Acta Geologica Sinica*, 85(4): 475–481(in Chinese with English abstract).
- Wedepohl K H. 1994. The composition of the continental crust[J]. *Mineralogical Magazine*, 58(7): 1217–1232.
- Wei Shaogang, Tang Juxing, Song Yang, Liu Zhibo, Wang Qin, Lin Bin, He Wen, Feng Jun. 2017. Petrogenesis, zircon U-Pb geochronology and Sr-Nd-Hf isotopes of the mid-acidic volcanic rocks from the Duolong deposit in the Bangonghu–Nujiang suture zone, Tibet, and its tectonic significance[J]. *Acta Geologica Sinica*, 91(1): 132–150(in Chinese with English abstract).
- Whalen J B, Currie K L, Chappell B W. 1987. A-type granites: geochemical characteristics, discrimination and petrogenesis[J].

- Contributions to Mineralogy & Petrology, 95(4): 407–419.
- Wright J B. 1969. A simple alkalinity ratio and its application to questions of non- orogenic granite genesis[J]. Geological Magazine, 106(4): 370–384.
- Wu Fuyuan, Sun Deyou, Li Huimin, Jahn B M, Wilde S. 2002. A-type granites in northeastern China: Age and geochemical constraints on their petrogenesis[J]. Chemical Geology, 187(1): 143–173.
- Wu Fuyuan, Jahn B M, Wilde S A, Lo Chinghua, Yui T F, Lin Qiang, Ge Wenchun, Sun Deyou. 2003. Highly fractionated I-type granites in NE China (I): Geochronology and petrogenesis[J]. Lithos, 66(3): 241–273.
- Wu Fuyuan, Li Xianhua, Yang Jinhui, Zheng Yongfei. 2007. Discussions on the petrogenesis of granites[J]. Acta Petrologica Sinica, 23(6): 1217–1238(in Chinese with English abstract).
- Wu Fuyuan, Liu Xiaochi, Ji Weiqiang, Wang Jiamin, Yang Lei. 2017. Highly fractionated granites: Recognition and research[J]. Science China: Earth Sciences, 47(7): 745–765 (in Chinese).
- Xiao W J, Windley B F, Huang B C, Han C M, Yuan C, Chen H L, Sun M, Sun S, Li J L. 2009. End-Permian to mid-Triassic termination of the accretionary processes of the southern Altaids: Implications for the geodynamic evolution, Phanerozoic continental growth, and metallogeny of Central Asia[J]. International Journal of Earth Sciences, 98(6): 1189–1217.
- Xu Wenliang, Pei Fuping, Wang Feng, Meng En, Ji Weiqiang, Yang Debin, Wang Wei. 2013. Spatial-temporal relationships of Mesozoic volcanic rocks in NE China: Constraints on tectonic overprinting and transformations between multiple tectonic regimes[J]. Journal of Asian Earth Sciences, 74: 167–193.
- Yan Shengwu, Bai Xianzhou, Wu Wenxiang, Zhu Bing, Zhan Qiongyao, Wen Long, Yang Hui, Wang Yuting. 2017. Genesis and geological implications of the Neoproterozoic A-type granite from the Lugu area, western Yangtze block[J]. Geology in China, 44(1): 136–150(in Chinese with English abstract).
- Yang Jinhui, Wu Fuyuan, Chung Sunlin, Wilde S A, Chu Meifei. 2006. A hybrid origin for the Qianshan A-type granite, northeast China: Geochemical and Sr-Nd-Hf isotopic evidence[J]. Lithos, 89(1): 89–106.
- Yang Jinhui, Wu Fuyuan, Chung Sunlin, Lo Chinghua, Wilde S A, Davis G A. 2007. Rapid exhumation and cooling of the Liaonan metamorphic core complex: Inferences from $^{40}\text{Ar}/^{39}\text{Ar}$ thermochronology and implications for Late Mesozoic extension in the eastern North China Craton[J]. Geological Society of America, 119(11/12): 1405–1414.
- Yang Qidi, Guo Lei, Wang Tao, Zeng Tao, Zhang Lei, Tong Ying, Shi Xingjun, Zhang Jianjun. 2014. Geochronology, origin, sources and tectonic settings of Late Mesozoic two-stage granites in the Ganzhuermiao region, central and southern Da Hinggan Range, NE China[J]. Acta Petrologica Sinica, 30(7): 1961–1981(in Chinese with English abstract).
- Yao Lei, Lü Zhicheng, Ye Tianzhu, Pang Zhenshan, Jia Hongxiang, Zhang Zhihui, Wu Yunfeng, Li Ruihua. 2017. Zircon U-Pb age, geochemical and Nd-Hf isotopic characteristics of quartz porphyry in the Baiyinchagan Sn polymetallic deposit, Inner Mongolia, southern Great Xing'an Range, China[J]. Acta Petrologica Sinica, 33(10): 3183–3199(in Chinese with English abstract).
- Yuan Honglin, Wu Fuyuan, Gao Shan, Liu Xiaoming, Xu Ping, Sun Deyou. 2003. Determination of U-Pb age and rare earth element concentrations of zircons from Cenozoic intrusions in northeastern China by laser ablation ICP-MS[J]. Chinese Science Bulletin, 48(22): 2411–2421.
- Yuan Honglin, Gao Shan, Dai Mengning, Zong Chunlei, Günther D. Fontaine G H, Liu Xiaoming, Diwu C R. 2008. Simultaneous determinations of U-Pb age, Hf isotopes and trace element compositions of zircon by excimer laser-ablation quadrupole and multiple-collector ICP-MS[J]. Chemical Geology, 247(1): 100–118.
- Zeng Qingdong, Guo Weikang, Chu Shaoxiong, Duan Xiaoxia. 2016. Late Jurassic granitoids in the Xilamulun Mo belt, Northeastern China: geochronology, geochemistry, and tectonic implications[J]. International Geology Review, 58(5): 588–602.
- Zhai Degao, Liu Jiajun, Wang Jianping, Yang Yongqiang, Liu Xingwang, Wang Gongwen, Liu Zhenjiang, Wang Xilong, Zhang Qibin. 2012. Characteristics of melt-fluid inclusions and sulfur isotopic compositions of the Hashitu molybdenum deposit, Inner Mongolia[J]. Earth Science—Journal of China University of Geosciences, 37(6): 1279–1290(in Chinese with English abstract).
- Zhai Degao, Liu Jiajun, Wang Jianping, Yang Yongqiang, Zhang Hongyu, Wang Xilong, Zhang Qibin, Wang Gongwen, Liu Zhenjiang. 2014. Zircon U-Pb and molybdenite Re-Os geochronology, and whole-rock geochemistry of the Hashitu molybdenum deposit and host granitoids, Inner Mongolia, NE China[J]. Journal of Asian Earth Sciences, 79(2): 144–160.
- Zhai Degao, Liu Jiajun, Stylianos Tombros, Anthony E Williams-Jones. 2017. The genesis of the Hashitu porphyry molybdenum deposit, Inner Mongolia, NE China: Constraints from mineralogical, fluid inclusion, and multiple isotope (H, O, S, Mo, Pb) studies[J]. Mineralium Deposita, 53(3): 377–397.
- Zhang Jiheng, Ge Wenchun, Wu Fuyuan, Liu Xiaoming. 2006. Mesozoic bimodal volcanic suite in Zhalantun of the Da Hinggan Range and its geological significance: Zircon U-Pb age and Hf isotopic constraints[J]. Acta Geologica Sinica, 80(1): 58–69.
- Zhang Jiheng, Gao Shan, Ge Wenchun, Wu Fuyuan, Yang Jinhui, Wilde S, Li Ming. 2010. Geochronology of the Mesozoic volcanic rocks in the Great Xing'an Range, northeastern China: Implications for subduction-induced delamination[J]. Chemical Geology, 276(3): 144–165.
- Zhang Ke, Nie Fengjun, Hou Wanrong, Li Chao, Liu Yong. 2012. Re-Os isotopic age dating of molybdenite separates from Hashitu Mo

- deposit in Linxi County of Inner Mongolia and its geological significance[J]. *Mineral Deposits*, 31(1): 129–138 (in Chinese with English abstract).
- Zhang Xuebing. 2017. Pb-Zn Polymetallic Deposits Metallogenetic Series and Prospecting Direction of the West Slope of southern Great Xing'an Range[D]. Changchun: Jilin University, 1–169(in Chinese with English abstract).
- Zhang Yutao, Zhang Lianchang, Ying Jifeng, Zhou Xinhua. 2006. Geochemistry of Zhalantun dyke swarm in north Da Hinggan Mountain and its geological implication[J]. *Acta Petrologica Sinica*, 22(11): 2733–2742(in Chinese with English abstract).
- Zhang Zhaochong, Mao Jingwen, Wang Yanbin, Pirajno F, Liu Junlai, Zhao Zhidan. 2010. Geochemistry and geochronology of the volcanic rocks associated with the Dong'an adularia-sericite epithermal gold deposit, Lesser Hinggan Range, Heilongjiang Province, NE China: Constraints on the metallogenesis[J]. *Ore Geology Reviews*, 37(3): 158–174.
- Zhao Yiming, Wu Liangshi, Bai Ge, Yuan Zhongxin, Ye Qingtong, Huang Minzhi, Rui Zongyao, Sheng Jifu, Lin Wenwei, Deng Songping, Mao Jingwen, Bi Chengsi, Dang Zefa, Wang Longsheng, Zhang Zuoheng, Chen Weishi. 2004. Metallogeny of the Major Metallic Ore Deposits in China[M]. Beijing: Geological Publishing House, 1–411(in Chinese).
- Zhou Xinmin, Sun Tao, Shen Weizhou, Shu Liangshu, Niu Yaoling. 2006. Petrogenesis of Mesozoic granitoids and volcanic rocks in South China: A Response to Tectonic Evolution[J]. *Episodes*, 29(1): 26–33.
- Zhou Zhenhua, Lü Linsu, Yang Yongjun, Li Tao. 2010. Petrogenesis of the Early Cretaceous A-type granite in the Huanggang Sn-Fe deposit, Inner Mongolia: Constraints from zircon U-Pb dating and geochemistry[J]. *Acta Petrologica Sinica*, 26(12): 3521–3537(in Chinese with English abstract).
- Zhu Rixiang, Xu Yigang. 2019. The subduction of the west Pacific plate and the destruction of the North China Craton[J]. *Science China: Earth Sciences*, 49(9): 1346–1356(in Chinese).
- Zhu Xinyou, Wang Jingbin, Wang Yanli, Cheng Xiyin, He Peng, Fu Qibin, Li Shunting. 2012. Characteristics of alkali feldspar granite in tungsten(tin) deposits of Nanling region[J]. *Geology in China*, 39(2): 359–381(in Chinese with English abstract).
- Zhu Xinyou, Zhang Zhihui, Fu Xu, Li Baiyang, Wang Yanli, Jiao Shoutao, Sun Yalin. 2016. Geological and geochemical characteristics of the Weilasito Sn-Zn deposit, Inner Mongolia[J]. *Geology in China*, 43(1): 188–208(in Chinese with English abstract).
- Zonenshain L P, Kuzmin M L, Natapov L M, Page B M. 1990. *Geology of the USSR: A Plate-tectonic Synthesis*[M]. Washington DC: American Geophysical Union, 1–242.
- Zorin Y A. 1999. Geodynamics of the western part of the Mongolia-Okhotsk collisional belt, Trans-Baikal region (Russia) and Mongolia[J]. *Tectonophysics*, 306(1): 33–56.
- ### 附中文参考文献
- 陈建林, 郭原生, 付善明. 2004. 花岗岩研究进展——ISMA花岗岩分类综述[J]. *甘肃地质*, (1): 67–73.
- 陈郑辉, 王登红, 盛继福, 应立娟, 梁婷, 王成辉, 刘丽君, 王永磊. 2015. 中国锡矿成矿规律概要[J]. *地质学报*, 89(6): 1038–1050.
- 陈志广, 张连昌, 吴华英, 万博, 曾庆栋. 2008. 内蒙古西拉木伦成矿带碾子沟钼矿区A型花岗岩地球化学和构造背景[J]. *岩石学报*, 24(4): 257–267.
- 管琪, 朱弟成, 赵志丹, 张亮亮, 刘敏, 李小伟, 于枫, 莫宣学. 2010. 西藏南部冈底斯带东段晚白垩世埃达克岩: 新特提斯洋脊俯冲的产物?[J]. *岩石学报*, 26(7): 2165–2179.
- 管育春, 杨宗锋, 薛新友, 邹滔, 程细音, 唐雷, 邓海辉. 2017. 内蒙古北大山杂岩体成因及其地质意义[J]. *矿产勘查*, 8(6): 1054–1068.
- 郭峰, 范蔚蔚, 王岳军, 林舸. 2001. 大兴安岭南段晚中生代双峰式火山作用[J]. *岩石学报*, 17(1): 161–168.
- 韩国卿, 刘永江, 温泉波, 李伟, 吴琳娜, 赵英利, 丁凌, 赵立敏, 梁琛岳. 2011. 西拉木伦河缝合带北侧二叠纪砂岩碎屑锆石LA-ICP-MS U-Pb年代学及其构造意义[J]. *地球科学——中国地质大学学报*, 36(4): 687–702.
- 贾小辉, 王强, 唐功建. 2009. A型花岗岩的研究进展及意义[J]. *大地构造与成矿学*, 33(3): 465–480.
- 李竞妍, 郭峰, 李超文, 李红霞, 赵亮. 2014. 东北地区晚古生代—中生代I型和A型花岗岩Nd同位素变化趋势及其构造意义[J]. *岩石学报*, 30(7): 1995–2008.
- 李真真, 秦克章, 赵俊兴, 李光明, 苏仕强. 2019. 锡-银多金属成矿系统的基本特征、研究进展与展望[J]. *岩石学报*, 35(7): 1979–1998.
- 林强, 葛文春, 曹林, 孙德有, 林经国. 2003. 大兴安岭中生代双峰式火山岩的地球化学特征[J]. *地球化学*, 32(3): 208–222.
- 林强, 葛文春, 吴福元, 孙德有, 曹林. 2004. 大兴安岭中生代花岗岩类的地球化学[J]. *岩石学报*, 20(3): 403–412.
- 刘家远. 2003. 复式岩体和杂岩体——花岗岩类岩体组合的两种基本形式及其意义[J]. *地质找矿论丛*, 18(3): 143–148.
- 刘锐, 杨振, 徐启东, 张晓军, 姚春亮. 2016. 大兴安岭南段海西期花岗岩类锆石U-Pb年龄、元素和Sr-Nd-Pb同位素地球化学: 岩石成因及构造意义[J]. *岩石学报*, 32(5): 1505–1528.
- 马星华, 陈斌, 赖勇, 鲁颖淮. 2009. 内蒙古敖伦花斑岩铜矿床成岩成矿年代学及地质意义[J]. *岩石学报*, 25(11): 247–258.
- 毛景文, 张作衡, 余金杰, 王义天, 牛宝贵. 2003. 华北及邻区中生代大规模成矿的地球动力学背景: 从金属矿床年龄猜测得到启示[J]. *中国科学: 地球科学*, 33(4): 289–299.
- 毛景文, 谢桂青, 张作衡, 李晓峰, 王义天, 张长青, 李永峰. 2005. 中国北方中生代大规模成矿作用的期次及其地球动力学背景[J]. *岩石学报*, 21(1): 171–190.
- 莫申国, 韩美莲, 李锦轶. 2005. 蒙古—鄂霍茨克造山带的组成及造山过程[J]. *山东科技大学学报(自然科学版)*, 24(3): 50–52.
- 邱检生, 肖娥, 胡建, 徐夕生, 蒋少涌, 李真. 2008. 福建北东沿海高分异I型花岗岩的成因: 锆石U-Pb年代学、地球化学和Nd-Hf同位

- 素制约[J]. 岩石学报, 24(11): 2468–2484.
- 邵济安, 张履桥, 牟保磊. 1998. 大兴安岭中南段中生代的构造热演化[J]. 中国科学(D辑), 28(3): 193–200.
- 邵济安, 李献华, 张履桥, 牟保磊, 刘玉琳. 2001a. 南口—古崖居中生代双峰式岩墙群形成机制的地球化学制约[J]. 地球化学, 30(6): 517–524.
- 邵济安, 刘福田, 陈辉, 韩庆军. 2001b. 大兴安岭—燕山晚中生代岩浆活动与俯冲作用关系[J]. 地质学报, 75(1): 56–63.
- 邵济安, 张履桥. 2002. 华北北部中生代岩墙群[J]. 岩石学报, 18(3): 312–318.
- 邵济安, 牟保磊, 朱慧忠, 张履桥. 2010. 大兴安岭中南段中生代成矿物质的深部来源与背景[J]. 岩石学报, 26(3): 649–656.
- 史长义, 鄂明才, 刘崇民, 迟清华, 胡树起, 顾铁新, 卜维, 鄂卫东. 2005. 中国花岗岩类化学元素丰度及特征[J]. 地球化学, 34(5): 56–68.
- 万乐, 刘正宏, 李刚, 辛后田. 2016. 内蒙古林西朝阳沟早白垩世花岗岩锆石U-Pb年代学和地球化学及其意义[J]. 地质与资源, 25(1): 1–10.
- 王京彬, 王玉往, 王丽娟. 2002. 大兴安岭南段中生代伸展成矿系统[J]. 矿床地质, (s1): 241–244.
- 汪洋. 2009. 北京白查A型花岗岩的地球化学特征及其成因与构造指示意义[J]. 岩石学报, 25(1): 13–24.
- 王永磊, 王登红, 张长青, 王成辉. 2012. 广西钦甲花岗岩体岩石地球化学特征及成因研究[J]. 岩石矿物学杂志, 31(2): 155–163.
- 韦少港, 唐菊兴, 宋扬, 刘治博, 王勤, 林彬, 贺文, 冯军. 2017. 西藏班公湖—怒江缝合带美日切错组中酸性火山岩锆石U-Pb年龄、Sr-Nd-Hf同位素、岩石成因及其构造意义[J]. 地质学报, 91(1): 132–150.
- 吴福元, 李献华, 杨进辉, 郑永飞. 2007. 花岗岩成因研究的若干问题[J]. 岩石学报, 23(6): 1217–1238.
- 吴福元, 刘小驰, 纪伟强, 王佳敏, 杨雷. 2017. 高分异花岗岩的识别与研究[J]. 中国科学: 地球科学, 47(7): 745–765.
- 鄂圣武, 白宪洲, 伍文湘, 朱兵, 詹琼窑, 文龙, 杨辉, 王玉婷. 2017. 扬子地块西缘新元古代泸沽A型花岗岩成因与变泥质岩熔融[J]. 中国地质, 44(1): 136–150.
- 杨奇获, 郭磊, 王涛, 曾涛, 张磊, 童英, 史兴俊, 张建军. 2014. 大兴安岭中南段甘珠尔庙地区晚中生代两期花岗岩的时代、成因、物源及其构造背景[J]. 岩石学报, 30(7): 1961–1981.
- 姚磊, 吕志成, 叶天竺, 庞振山, 贾宏翔, 张志辉, 吴云峰, 李睿华. 2017. 大兴安岭南段内蒙古白音查干Sn多金属矿床石英斑岩的锆石U-Pb年龄、地球化学和Nd-Hf同位素特征及地质意义[J]. 岩石学报, 33(10): 3183–3199.
- 翟德高, 刘家军, 王建平, 杨永强, 刘星旺, 王功文, 柳振江, 王喜龙, 张琪彬. 2012. 内蒙古哈什吐钼矿床熔融-流体包裹体特征及硫同位素组成[J]. 地球科学——中国地质大学学报, 37(6): 1279–1290.
- 张可, 聂凤军, 侯万荣, 李超, 刘勇. 2012. 内蒙古林西县哈什吐钼矿床辉钼矿铼-锇年龄及其地质意义[J]. 矿床地质, 31(1): 129–138.
- 张雪冰. 2017. 大兴安岭南段西坡铅锌多金属矿床成矿系列与找矿方向[D]. 长春: 吉林大学, 1–169.
- 张玉涛, 张连昌, 英基丰, 周新华. 2006. 大兴安岭北部扎兰屯脉岩群的地球化学特征及其地质意义[J]. 岩石学报, 22(11): 2733–2742.
- 赵一鸣, 吴良士, 白鸽, 袁忠信, 叶庆同, 黄民智, 范宗瑶, 盛继福, 林文蔚, 邓颂平, 毛景文, 毕承恩, 党泽发, 王龙生, 张作衡, 陈伟十. 2004. 中国主要金属矿床成矿规律[M]. 北京: 地质出版社, 1–411.
- 周振华, 吕林素, 杨永军, 李涛. 2010. 内蒙古黄岗锡铁矿区早白垩世A型花岗岩成因: 锆石U-Pb年代学和岩石地球化学制约[J]. 岩石学报, 26(12): 3521–3537.
- 朱日祥, 徐义刚. 2019. 西太平洋板块俯冲与华北克拉通破坏[J]. 中国科学: 地球科学, 49(9): 1346–1356.
- 祝新友, 王京彬, 王艳丽, 程细音, 何鹏, 傅其斌, 李顺庭. 2012. 南岭锡钨多金属矿区碱长花岗岩的厘定及其意义[J]. 中国地质, 39(2): 359–381.
- 祝新友, 张志辉, 付旭, 李柏阳, 王艳丽, 焦守涛, 孙雅琳. 2016. 内蒙古赤峰维拉斯托大型锡多金属矿的地质地球化学特征[J]. 中国地质, (1): 188–208.